THE ROLE OF LOESS WEATHERING IN THE GROUNDWATER CHEMISTRY OF THE CHACO-PAMPEAN PLAIN (ARGENTINA)

Armengol, S.[a,b], Ayora, C. [c], Manzano, M.[d], Bea, S. A. [a,b], Martínez, S. [e]

[a] Consejo Nacional de Investigaciones Científicas y Técnicas (CONICET), Av. Rivadavia 1917, C1033AAJ Ciudad Autónoma de Buenos Aires, Argentina.

[b] Instituto de Hidrología de Llanuras "Dr. Eduardo J. Usunoff", Av. República Italia 780, 7300 Azul, Buenos Aires, Argentina.

[c] Instituto de Diagnóstico Ambiental y Estudios del Agua (IDAEA-CSIC), C/ Jordi Girona 18, 08034 Barcelona, España.

[d] Escuela de Ingeniería de Caminos, Canales y Puertos y de Ingeniería de Minas, Universidad Politécnica de Cartagena, P° de Alfonso XIII 52, E-30203 Cartagena, España.

[e] Autoridad de Cuenca Matanza Riachuelo (ACUMAR), Esmeralda 255 PB, C1033AAJ Ciudad Autónoma de Buenos Aires, Argentina.

Abstract

The Chaco-Pampean Plain (CPP), Argentina, is one of the most extensive loess areas in the world, higlhly productive in terms of agriculture and livestock and with a generalized groundwater signature of Na-HCO_3 water type. High As concentrations have been often reported in aquifers throughout the entire CPP related to higher pH and alkalinity values. The processes leading to the groundwater from the humid Matanza-Riachuelo Aquifer System (MRAS) to acquire its alkalinity and pH have been investigated by means of detailed sampling of water and solid phases and geochemical modeling (Phreeqc code). The model has also been applied to two extra areas of the CPP with different climates: the semi-arid Río Dulce Alluvial Aquifer (RDA), and the arid Northern area of the La Pampa province (NLP). The analyses of groundwater from the three

different regions (from humid to arid) confirm the positive correlation between arsenic and the high pH and HCO_3 concentrations. The model has offered insights into key soil-rock interaction parameters that determine the groundwater chemistry of the CPP. Thus, in addition to the already known calcite precipitation, Ca retention by the volcanic glass exchange complex has appeared as crucial for groundwater to acquire the characteristic Na-HCO_3 signature. Moreover, the model has also highlighted the role of low CO_2 pressures in attaining the high pH values measured in poorly vegetated soils. Of particular significance is the unexpected role played by the formation of secondary alumino-silicates in increasing (rather than decreasing) pH. Further investigations on the role of volcanic glass in the soil exchange properties and the chemical composition of the exchange complex together with the accurate determination of the clay mineralogy are needed to understand the high pH and alkalinity values of groundwater of this vast region.

Keywords: loess, geochemical modeling, dissolution kinetics, cation exchange, volcanic glass, arsenic

1 Introduction

The Chaco-Pampean Plain (CPP) covers an area of 10^6 km^2 and extends from the border with Paraguay in the North to the Patagonian Plateau in the South (Figure 1). The CPP is the largest loess deposit in South America and has become the most productive zone as regards agriculture and livestock. Most of the CPP terrain is flat, with the exception of some parts of Córdoba and Tucumán Provinces. Loess sediments are Pleistocene-Holocene deposits formed by accumulations of wind-blown particles (Teruggi, 1957; Iriondo, 1997, Zárate, 2003). Northern

loess sediments (20°S - 37°S) originated in the glaciers of the south central Andes (25°S - 34°S), the Paraná basalts and the Puna Altiplano (Smith et al., 2003). The mineral compositon of the loess has been described in earlier studies (Teruggi, 1957; González Bonorino, 1965; Tófalo et al., 2005; Bonorino et al., 2008). These authors established that the loess is mainly made up of plagioclase, quartz, K-feldspar, volcanic glass, pyroxene, amphibole, calcite, and the clay fraction of montmorillonite and illite. According to Zink and Sayago (1999) and Scopa (1976), even if the conditions remain unclear, the presence of montmorillonite is likely to be related to processes of clay neoformation.

The chemical composition of the groundwater of the CPP is mainly of the Na-HCO_3 water-type, with neutral to alkaline pH (pH = 6.6 to 8.9). This groundwater chemistry signature has been attributed to both the loess composition and the water transit through the unsaturated zone (UZ) (Armengol et al., 2017; Smedley et al., 2002). Concentrations of As exceeding the WHO guidelines (10 µg L^{-1}) have been documented in groundwater of many localities of the CPP (see Smedley and Kinninburg, 2002; Farías et al., 2003; Blarasin, 2003; Bundschuh et al., 2004, 2008; Fernández Turiel et al., 2005; Bhattacharya et al., 2006; Blanes et al., 2006; Guber et al., 2009; Nicolli et al., 2012). In the CPP the highest concentrations of As (more than 1 mg L^{-1}) are found in HCO_3-Na type groundwater with neutral to high pH (Garcia et al., 2007; Borzi et al., 2015; Nicolli et al., 2012; Vital et al., 2019).

The CPP fine textured Quaternaty loess-type sediments with interbedded volcanic ash is thought to be the primary source of As (Bundschuh et al., 2004; Nicolli et al., 2012; Raychowdhury et al., 2014). However, many authors found no regional relationship between the As contents of the sediments and the groundwater As content (Blanco et al., 2006; Paoloni et al., 2002, 2005; Fiorentino et al., 2007). That is because the release to the aqueous phase from silicate weathering comprising the loess-type sediments occurs if no sorption processes retained As onto oxides. The strong adsorptive capacity onto the surface of Al, Fe and Mn-oxides and hydro-

oxides is a key process of As mobilization. Under oxic environments As(V) desorption occurs at pH values higher than 8, increasing the arsenic concentration. in the groundwater (Dzombak and Morel, 1990). Indeed, in neutral to alkaline water, the predominant aqueous species of As(V) is the anion $HAsO_4^{2-}$and it is increasingly desorbed from Al, Mn and Fe hydro-oxides by the competence of OH^- and HCO_3^- (Smedley et al., 2002; So et al., 2008; Gao et al., 2011). Therefore, the presence of As of geogenic origin in groundwaters of the CPP is mainly controlled not only by the As content of the primary lithologies, but by the groundwater chemistry conditions such as pH and alkalinity. It is well known that the highest concentrations of As (more than 1 mg/L) in this region are found in groundwater systems with fine textured Quaternay loess-type sediments with neutral to high pH and a HCO_3-Na groundwater type (Garcia et al., 2007; Nicolli et al., 2012; Bozi et al., 2015; Vital et al., 2019).

This paper seeks to generate knowledge about how shallow groundwater acquires its chemical properties in the Chaco-Pampean Plain, particularly its Na-HCO_3 water type, pH and alkalinity values. To this end, a geochemical model addresses the main processes involved in the chemistry of shallow groundwater that is the leading processes taking place during rainwater infiltration to the water table (rainfall, evapoconcentration, mineral dissolution/precipitation, cation exchange). The results of the model are compared with the shallow groundwater chemistry from the MRAS and later with the arid Northern area of the La Pampa province (NLP) and the Río Dulce Alluvial Aquifer (RDA). These two extra areas of the CPP undergo very different climatic conditions and recorded As concentrations up to 4.9 and 13.5 mg/L, respectively.

2 Materials and methods

2.1 Area of study

The Matanza-Riachuleo Aquifer System (MRAS) is characteristic of the humid Pampa, with an annual rainfall of 1236 mm and a mean temperature of 18 ^oC. The MRAS is the most productive zone of the country dedicated to cattle rearing and the production of soyabean, maize and

wheat. The Matanza-Riachuelo Aquifer System (MRAS) covers an area of 2000 km^2 of the Buenos Aires Province (Armengol et al., 2017). (Figure 1).

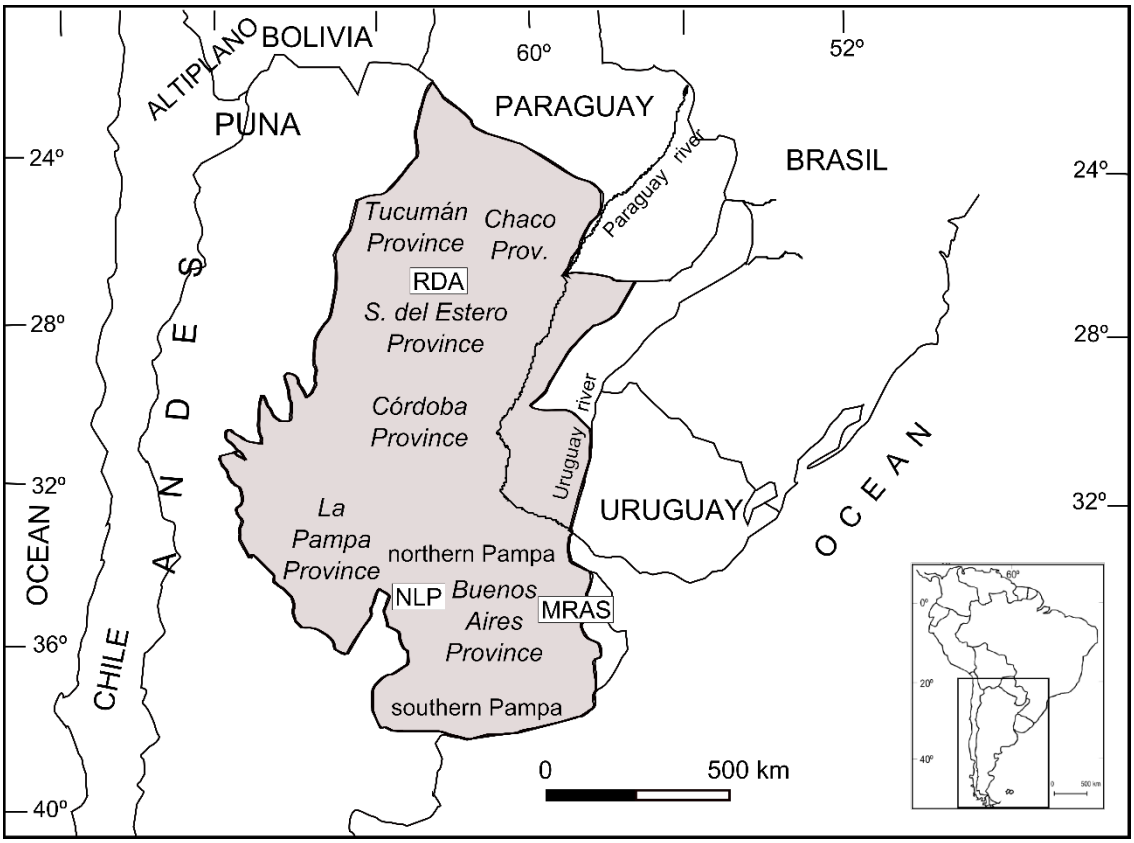

Figure 1. Map of the Chaco-Pampean Plain with the geographical domains, mountain ranges and the location of the study areas. RDA: Río Dulce alluvial aquifers in Santiago del Estero Province (Bhattacharya, 2006; Sifuentes and Nordberg, 2003). NLP: Northern area of the La Pampa province (Smedley et al., 2002). MRAS: Matanza-Riachuelo Aquifer System in Buenos Aires Province (Armengol et al., 2017).

The study was complemented with literature analyses from two more CPP regions with different climatic conditions (Figure 1). The Northern area of the La Pampa province (NLP) is arid, with an annual rainfall of 746 mm and a mean temprerature of 15 ^{o}C. Vegetation is scarce, although grassland for cattle rearing coexists with some grain crops. The aridity is due to the high evaporation during the dry season (May – September), which results in the absence of perennial streams. Superficial water bodies are limited to the wet season (October – April) when small lagoons are filled with water. In the dry season, salt deposits develop around these ephemeral water bodies because of the high evaporation (Smedley et al., 2002). The groundwater samples belong to 15 public water-supply boreholes, private boreholes or hand-dug wells from 150 m to

over 20 m in depth (Table S5; Figure 1). The NLP covers an area of 7700 km^2, North of Santa Rosa. The hydrochemical data were extracted from Smedley et al. (2002).

The Río Dulce Alluvial Aquifer (RDA) has a semi-arid climate with a rainfall of 532 mm with hot rainy summers and cold dry winters. The groundwater sampled extended over 1500 km^2 in the province of Santiago del Estero. Thirty samples of Na-HCO_3 water type were selected from shallow wells (1.9 m to 18 m in depth). Despite its low rainfall, the evaporation is not as high as in the Northern area of the La Pampa province (NLP). The hydrochemical data are extracted from Sifuentes and Nordberg (2003) (Table S5; Figure 1). The chemistry of the RDA groundwater samples shows a considerable variation that could result from excessive irrigation in some areas (Battacharya et al., 2006). This variation of groundwater chemistry may be attributed to the environmental differences between the alluvial cone covered with grassland and the occasional clumps of native trees in the surrounding areas. The area has also suffered from deforestation due to agriculture (Boletta et al., 2006).

2.2 General hydrochemistry

The chemical composition of the groundwater of the Chaco-Pampean Plain is mainly of the Na-HCO_3 water-type with neutral to alkaline pH (pH = 6.6 to 8.9). This groundwater chemistry has been traditionally attributed to the composition of the loess and to the passage of the water though the unsaturated zone (Logan et al., 1999; Martínez and Bocanegra, 2002; Smedley et al., 2002; Zabala et al., 2015; Armengol et al., 2017). Raychowdhury et al. (2014) developed a focused on the origin of As in the NLP region, and, in addition to the silicate weathering, they attributed high Na and HCO_3 concentrations to mixing with brakish or evapoconcentrated water. Some specific areas of the MRAS, RDA and the NLP regions have recorded NaCl and CaNa-SO_4Cl groundwater types achieving relatively high Cl and SO_4 concentrations (up to 2000 and 1000 mg L^{-1}, respectively). However, these specific groundwater types are mainly influenced by small scale rather than large scale processes such as groundwater salinization due to encroached

142 saline waters (Armengol et al., 2017), high evaporation rates (Smedley et al., 2002), irrigation
143 (Sifuentes and Nordberg, 2003) and evaporite mineral dissolution (Logan et al., 1999; Smedley
144 et al., 2002; Armengol et al., 2017). The present study incorporates the evapoconcentration
145 process due to its relevance for the final groundwater chemistry.

146 The consensus of opinion seems to be that the groundwater flow inside the CPP aquifers is slow.
147 Thus, to cross a distance of 100 km, Smedley et al. (2002) estimated 10 ky and Bundschuh et al.
148 (2004) 13 to 40 ky. However, recent radiocarbon and ^{3}H studies from the southern part of the
149 CPP indicate an age younger than 50 yr for the shallow groundwaters (Smedley et al., 2002;
150 Martinez et al., 2017). This short time span has been attributed to the time taken by the water
151 to cross the unsaturated zone. This is consistent with the infiltration rates and the thickness of
152 the usaturated zone described for the three study areas. Thus, Smedley et al. (2002), Bundschuh
153 et al. (2004) and IHLLA (2012) reported infiltration rates of 30, 50 to 100 and 134 mm y^{-1} for NPL,
154 RDA and MRAS regions, respectively. For an average porosity of 0.5, the water can reach depths
155 between 1 and 15 m in 50 years, which are similar to those of the unsaturated zone in the three
156 areas.

157 2.3 Sampling and analytical

158 Groundwater samples were collected from 18 piezometers at different depths down to 20 m in
159 March – April 2014 by the Instituto Nacional del Agua (INA, Argentina). The boreholes belong to
160 a monitoring network of the Autoridad de Cuenca Matanza Riachuelo (ACUMAR). Sampling
161 followed the INA protocol, which includes borehole purging, on-site measuring of pH and
162 electrical conductivity (EC, μS cm^{-1}) inside a flow-through cell, filtering (0.45 μm) and acidifying
163 (pH<2) samples for trace components, refrigerated transport to the laboratory and rapid
164 analysis. Alkalinity (quoted in this paper as HCO_3 equivalent) was also measured on-site
165 Groundwater chemical components (Ca, Mg, Na, K, Cl, HCO_3, SiO_2, Al, As), pH and EC were also
166 analyzed at the INA laboratory following the methodology proposed by the American Public

Health Association (APHA, 2005). For an easier reading of this text, the electric charge of the ions has been omitted.

An atmospheric precipitation network of the Matanza-Riachuelo Aquifer System was created for this study. The precipitation network consisted of six samplers distributed along the entire basin. Samplers were designed following the model recommended by the International Atomic Energy Agency (Gröning et al., 2012). Rainwater samples were collected monthly, filtered (0.20 µm nylon) and stored in black polyethylene large cans. After the analysis every four months cans were pre-cleaned with deionized water. The sample collection lasted for three years (2015-2017). The chemical components used for this work (Ca, Mg, Na, K, Cl, HCO_3, SiO_2, Al), pH and EC were analyzed at the Instituto de Hidrologia de Llanuras (IHLLA) located in Azul (Argentina) also according to APHA method (APHA, 2005).

Sediment samples were collected at different depths (from 0 to 10 m) from a borehole (Lat. -35.001159º; Long. -58.631155º) drilling the Pampeano Sediments at the upper basin of the MRAS. Total and clay-size fraction mineralogy were analyzed from 20 sediment samples by a PANalytical X'Pert PRO X-ray powder diffractometer equipped with a sealed proportional detector with Cu Kα radiation at 45 kV, 40 mA. The sediment granulometry was analyzed by a Mastersizer laser diffraction particle size ananlyzer. Both analyses were performed at the Universidad Nacional de la Plata (UNLP, Argentina). Measured Cation Exchange Capacity (CEC) and the concentration of exchangeable bases (i.e., CaX_2, MgX_2, KX, NaX) from 8 selected sediment samples (6 silt, 1 clay and 1 silty-clay sized samples) were performed according to the SAMLA (2004) protocol at the Laboratorio de Analisis de Suelos de la Facultad de Agronomía (Azul, Argentina). The exchangeable bases were extracted from the soil using a 1 N NH_4Ac, pH 7 or 8.2 solution (the latter solution was used for samples with reaction to HCl 10% v/v, indicating the presence of carbonates). The CEC was quantified by displacing the NH_4 by 1N NaAc solution.

3 Geochemical modeling

192 The modeling seeks to describe the processes driving the chemical evolution from rainwater to
193 shallow groundwater of the CPP thought the study of the MRAS (Figure 2). The conceptual model
194 domain corresponds to the UZ, and the water input in this system is evapoconcentrated
195 rainwater (i.e, concentrated to reproduce the effect of evapotranspiration on the solute
196 concentrations before and during infiltration). Water evolved chemically after reacting with the
197 edaphic CO_2 and loess minerals (Figure 2). Modeled UZ was considered as a whole (0D rather
198 than 1D model) due to the absence of chemical data vertically distributed at different depths.
199 The model included cation exchange processes in addition to mineral dissolution under kinetic
200 rate laws and precipitation under local equilibrium assumption. The chemical compositions
201 calculated were compared with those measured in the shallow groundwaters. Calculations were
202 performed with the code PHREEQC (Parkhurst and Appelo, 1999) considering water-mineral
203 reactions in a close system. Equilibrium was assumed for aqueous speciation, cation exchange,
204 gas dissolution and mineral precipitation reactions, whereas mineral dissolution reactions were
205 computed under kinetic laws. Systematic runs of the PHREEQC code modifying the parameters
206 and the graphical representations were performed with the GibbsStudio software (Nardi and de
207 Vries, 2017).

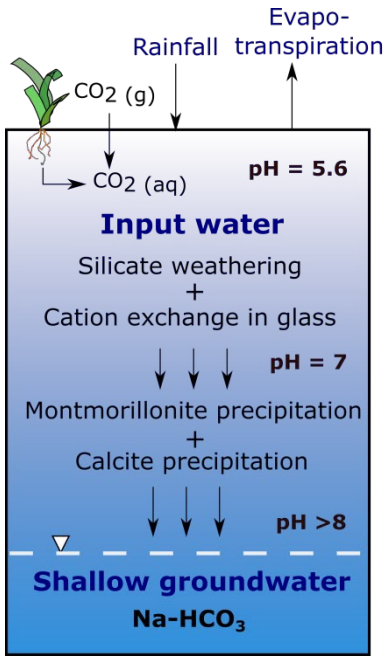

Figure 2. Conceptual model of the Chaco-Pampean Plain unsaturated zone (UZ) processes.

3.1. Initial primary and secondary minerals

The X-ray diffraction analyses carried out in 20 samples from a MRAS borehole indicate that the loess minerals in the total sample are quartz, plagioclase, potassium feldspar, calcite and pyroxene (traces). Illite (I), smectite (S) and the interlayered I/S association are the most abundant minerals in the clay-size fraction. However, the glass scattered throughout the sediments could not be identified by X-ray diffraction, and a quantitative assessment of the mineral proportions by Rietveld method was discarded. The chemical composition of glass was computed using the wt% of SiO_2, Al_2O_3, Fe_2O_3, FeO, MgO, CaO, Na_2O, K_2O, TiO_2, and MnO from three different studies (Nicolli et al., 1989, 2010 and Shultz, 2004). Since their mineralogical description was very similar, the mass of the minerals was deduced from the average oxide concentration in loess bulk samples reported in González-Bonorino (1965), Smedley et al. (2005) and Nicolli et al. (1989), for the MRAS, RDA and NLP, respectively (Table S1). Using a simplified approximation of the CIPW norm (Cohen and Ward, 1991; Rosen et al., 2004), the molar elemental proportions including glass were used to assign the Si, Fe, Mg, Ca, Na, K, Mn and C mass to the different mineral phases of the loess (Table 1).

However, prior to perform this normative distribution of the chemical analysis, the composition of each mineral phase had to be determined. Thus, andesine, $Na_{0.6}Ca_{0.4}Al_{1.4}Si_{2.6}O_8$, and hyperstene, $MgSi_3O_8$, were selected as representative phases for plagioclase and pyroxene groups, respectively (Nicolli et al., 1989, 2012); for the clay fraction, a montmorillonite of composition $Ca_{0.17}Al_{2.33}Si_{3.67}O_{10}(OH)_2$ was selected (González-Bonorino, 1965). The chemical composition of the glass, $Na_{1.3}K_{0.8}Mg_{0.4}Ca_{0.4}Fe(III)_{0.3}Al_{2.6}Si_{11.5}O_{29.0}$, was obtained as an average of volcanic glass grains separated manually from the loess (Nicolli et al., 1989, 2010; Schultz, 2004). These analyses reveal an alumino-silicate composition with Na as a main cation regardless of the origin of the samples (Table S2). Thus, taking into account the stoichiometry of each mineral, Mg+Fe(II)+Mn, Fe(III) and C(IV) were directly transformed into hyperstene, goethite and calcite, respectively. In order to obtain volume proportions similar to those reported in the literature (Bundschuh, 2004; Nicolli, 1989), Na mass was arbitrarily assigned to andesine (3/4) and glass (1/4), and K was assigned to K-feldspar (2/3) and Illite (1/3). The remaining Si was assigned to quartz. This simple normative calculation resulted in an imbalance of Al and Ca below 10% of the total amount, which was considered satisfactory. The estimated mass of each mineral (mol kg^{-1} rock) was transformed into PHREEQC input concentrations (mol kgw^{-1}) assuming a loess porosity of 0.45 (Rinaldi et al., 2007; Weinzettel et al., 2005) and densities of 1 and 2.6 g cm^{-3} for the aqueous and average solid phases, respectively (Table 1).

Table 1. Mineral concentrations of the three loess regions considered in the model. Legend: M= mineral concentration in mol kg^{-1} loess; Vf= volume fraction; m0= mineral concentration in mol L^{-1} of pore water; A= surface area calculated for a total rock surface area of 100 m^2 kgw^{-1} (S_{rock}).

		RDA				NLP				MRAS			
		M	Vf	m0	A	M	Vf	m0	A	M	Vf	m0	A
hyperstene	$(Mg,Fe(II),Mn)SiO_3$	0.049	0.05	1.550	17.7	0.046	0.04	1.456	16.1	0.027	0.03	0.872	11.9
glass	$Na_{1.3}K_{0.8}Mg_{0.4}Ca_{0.4}Fe(III)_{0.3}Al_{2.6}Si_{11.5}O_{29.2}$	0.024	0.21	0.763	47.2	0.021	0.18	0.678	41.3	0.021	0.19	0.675	42.9
andesine	$Na_{0.6}Ca_{0.4}Al_{1.4}Si_{2.6}O_8$	0.108	0.35	3.435	65.2	0.096	0.29	3.051	57.1	0.096	0.30	3.038	59.3
calcite	$CaCO_3$	0.000	0.00	0.000	0.0	0.000	0.00	0.000	0.0	0.006	0.01	0.186	4.7
goethite	FeOOH	0.056	0.04	1.774	14.7	0.050	0.03	1.600	13.0	0.052	0.03	1.641	13.8
K-feldspar	$KAlSi_3O_8$	0.022	0.08	0.698	23.8	0.036	0.12	1.132	31.2	0.021	0.07	0.671	22.9
illite	$K_{0.6}Mg_{0.25}Al_{2.3}Si_{3.5}O_{10}(OH)_2$	0.011	0.05	0.349	17.7	0.018	0.08	0.566	23.1	0.011	0.05	0.335	17.0
montmor.	$Ca_{0.17}Al_{2.33}Si_{3.67}O_{10}(OH)_2$	0.000	0.00	0.000	0.0	0.000	0.00	0.000	0.0	0.000	0.00	0.000	0.0
quartz	SiO_2	0.307	0.22	9.758	48.6	0.378	0.26	12.017	53.0	0.452	0.32	14.358	62.1

Grain-size analysis of eight shallow samples from the MRAS aquifers reported in average 68% of silt (4 - 62.5 µm), 19% of sand (>62.5 µm) and 13% of clay (<4µm) (Table 2). These results agree with those reported by the Instituto Nacional de Tecnología Agropecuaria, Argentina (INTA, 1979) where the 70% of loess was composed of silt, around 20% of clay, and 5-15% of sand particles. There is a decreasing SW to NE trend in grain-size from sandy to clayey loess attributed to three successive deposition belts (Morrás and Cruzate, 2000), being the easternmost belt close to the Paraná–Río de La Plata axis (Zárate, 2003).

Table 2. Eight grain size analyses from 0 to 10 m depth samples from the Matanza-Riachuelo Aquifer System sediments.

Depth	Clay	Silt	Coarse silt	Total silt	very fine sand	Fine sand	Medium sand	Total sand
m	0 - 3.9 µm	3.9 - 31 µm	31 - 62.5 µm	% total	62.5 - 125 µm	125 - 250 µm	250 - 500 µm	% total
0.07	13.73	50.06	18.65	68.71	14.89	2.68	0	17.57
0.23	15.16	53.37	19.7	73.07	10.21	1.57	0	11.78
0.4	11.65	42.37	25.29	67.66	18.14	2.55	0	20.69
1.16	11.65	36.09	23.16	59.25	24.56	4.63	0	29.19
2.41	16.66	64.76	12.87	77.63	5.33	0	0	5.33
4.53	15.78	61.73	18.31	80.04	4.11	0.07	0	4.18
7.44	12.06	37.54	33.48	71.02	16.84	0.08	0	16.92
9.12	8.84	26.77	20.57	47.34	20.55	11.08	10.82	42.45

However, for the general modeling pourposes of this work, the surface area was approximated by considering loess as an ensemble of coarse silt sized (31 µm) spheres, which is equivalent to a total rock surface area of 100 m^2 kgw^{-1} for a porosity of 0.45 (Table 1). Then, the reactive surface area of each mineral was assessed by distributing the total surface area according to the volume fraction of each mineral powered to 2/3 (Table 1). Nevertheless, the total rock surface area in contact with water and, therefore, participating in the reactions is a highly uncertain parameter and will be discussed below (sections 3.5.5 and 4.3.1.).

3.2. Soil CO_2

Direct measurements of CO_2(g) in UZ were not carriet out in the MRAS, and no data are recorded in the literature for RDA and NLP. Brook et al. (1983) revealed direct increase in the CO_2 pressure with vegetation recording CO_2 measurements in the soil during the growing season in 19 regions from nine countries. In the absence of measurements in the areas considered, the CO_2 pressures

in the soil were assumed to agree with those of other authors in areas of similar vegetation. Thus, a high CO_2 pressure of 10^{-2} bar was assumed for the MRAS and the RDA areas. The MRAS soils are intensively used for agriculture implying a higher root respiration rate and intensive microbiological activity. The RDA is located in a semi-arid region, where the groundwater samples were taken from an alluvial cone covered with bushes and grassland. Finally, given the scarcity of vegetation cover in the NLP, the CO_2 pressure approximated the atmospheric value ($10^{-3.5}$ bar). Since CO_2 pressure of the soil is also known to vary with the temperature and moisture content, the uncertainty of this parameter was high and varied between seasons. Therefore, a sensitive analysis of the effect of CO_2 pressure on groundwater composition was performed (section 4.3.1).

3.3. Cation exchange capacity (CEC)

The CEC was measured in 8 sediment mostly silt-sized samples taken from 0 to 10 m depth in a borehole at the MRAS upper basin (Table 3). The exchange complexes are rich in Ca and Mg, and poor in K and Na.

Table 3. Total CEC and composition of the exchange complex in 8 sediment samples at different depths from the Matanzas-Riachuelo Aquifer System (in meq 100 g^{-1} soil).

Depth (m)	CEC	Ca	Mg	K	Na
0-0.3	14.2	9.1	2.3	2.1	0.1
0.4-0.7	25.7	13.6	7.5	4.3	0.2
0.7-1	24.4	14.2	6.7	2.5	0.4
1-2	15.7	12.3	7.1	1.9	0.6
2-3	20.5	16.4	10.7	2.9	0.4
4-5	28.8	17.9	13.1	2.6	0.5
7-8	33.4	19.9	16.1	3.2	0.7
9-10	25.8	17.5	10.4	2.8	0.6

All the known studies throughout the Chaco-Pampean Plain have recorded CEC values ranging from 15 to 35 meq 100 g^{-1} soil (Zinck and Sayago, 1999; Martínez and Bocanegra, 2002; Aullóon, 2013, Zabala et al., 2016). This is of significance when compared with the minor role played by exchangeable clays (less than 10% in mineral volume, including illite and montmorillonite). Moreover, Aullón (2013) found similar CEC values (21.84 meq 100g^{-1} soil) in volcanic ash

291 composed of approx. 90% of glass. Furthermore, Paul (1977) reported that alkali and alkali-earth
292 cations were easily extracted from glass with acid solutions. This extraction was practically
293 instantaneous and did not correlate with the silica concentration in solution (below detection
294 limits). Therefore, despite its dissolution, the glass fraction of loess has been regarded as the
295 exchanger in the model. Indeed, as described below (section 3.5.3), glass dissolution is very slow
296 compared to cation exchange (assumed instantaneous in the calculations). Therefore, the
297 structure of the glass would be supported by the Si-O bonds as exchange proceeds in the bulk
298 of the solid and only a very tiny amount of surface dissolves.

299 Unlike the CEC values, the chemical composition of the exchange complex (ECC) has scarcely
300 been investigated, and data from only two localities from the Province of Buenos Aires ("Humid
301 Pampas") are available. The ECC data consisted on average of 8 samples from 0 to 10 m depth
302 from the MRAS (Table 3) and 15 samples from 3 to 32 m depth from the Del Azul Creek Basin
303 (Zabala et al., 2016, Table S4). The exchange complexes are rich in Ca and Mg, and poor in K and
304 Na. The average composition of the exchange complex of the two localities was 17.6, 10.7, 2.1
305 and 2.0 meq 100 g^{-1} soil for CaX_2, MgX_2, NaX and KX, respectively, with a total CEC of 25.3 meq
306 100 g^{-1} soil. These values were used as the initial condition of the model and the total CEC value
307 has been considered during the simulations.

308 ## 3.4. Boundary water input

309 The composition of input water (infiltrating water) was assessed by standard rainwater
310 chemistry and a concentration factor (c_f). The standard rainwater chemistry was approximated
311 by a 2015-2017 average from the Matanza-Riachuelo River Basin. The solute concentration in
312 rainwater was increased by a coefficient c_f because of evapotranspiration. The final input water
313 was the result of applying the c_f of each study area (MRAS, RDA, and NLP) to the solute
314 concentrations of rainwater in the MRAS (Table 4). Assuming that Cl behaves conservatively in

315 water-rock interactions, the c_f consisted in the ratio of the average Cl concentration in
316 groundwater and the average Cl in rainwater.

317 The calculated c_f was 8, 26 and 58 for the MRAS, RDA and NLP areas, respectively. As expected,
318 the lowest c_f was obtained for the MRAS "Humid Pampas" because of its rainfall that exceeds
319 1200 mm yr^{-1}. By contrast, the highest c_f was obtained for the NLP, which was consistent with
320 the arid climate of the "Dry Pampas" where high temperatures over 40 °C with strong winds
321 were achieved during the dry-season (Aullón, 2013). In order to reduce the potential influence
322 of the secondary halite dissolution process in this region, the c_f was computed with the first
323 quartile of the data (1Q) instead of with the median value. The influence of the rainwater
324 chemistry and the c_f in the composition of groundwater is discussed below (section 4.2).

325 Table 4. Average chemical composition of rainwater (first row) and calculated infiltrating water for the three study
326 areas (mg L^{-1}) (rows 2 to 4).

	pH	Ca	Mg	Na	K	C	Cl	Si
Rainwater 2015-2017	5.6	3.9	0.6	2.9	1.7	13.4	1.9	1.2
Input water MRAS	5.6	30.4	5.1	23.0	13.5	105.5	15.1	9.8
Input water RDA	5.6	102.1	17.0	77.4	45.4	354.8	50.6	33.0
Input water NLP	5.6	222.6	37.1	168.8	99.0	773.9	110.4	72.0

327

328

329 ## 3.5. Reaction rates and constants

330 ### 3.5.1. Thermodynamic data

331 The thermodynamic equilibrium constants for aqueous speciation and for gas and mineral-water
332 reactions were extracted from the Wateq4f data base (Ball and Nordstrom, 1991). The solubility
333 product of andesine was calculated using an ideal solid-solution model (Equation 1).

$$\text{Log K} = \sum_{i}^{n} (x_i \log K_i + x_i \log x_i) \quad (1)$$

334 where n is the number of end-members, x_i is the molar fraction and K_i is the equilibrium constant
335 of the i-th end-members, albite and anortite in this case. Clinoenstatite was used as a proxy for
336 pyroxene.

No thermodynamic data were available for the glass fraction of the loess. To estimate the value, the glass was considered an ideal solid solution of oxides (Paul, 1977). Therefore, the solubility product of the glass was obtained with Equation 1 and x_i and K_i were extracted from the LLNL database of the PHREEQC software package (Johnson et al., 2000). This method has been satisfactorily used to describe the behaviour of borosilicate and aluminosilicate glasses (Bourcier et al., 1992; Ménard et al., 1998; Leturcq et al., 1999), and to estimate the solubility product of basaltic glass (Techer et al., 2001; Aradóttir et al., 2013). The mineral-water reactions included in the calculations and their log K values at 25 °C are listed in Table 5.

345 Table 5. Reaction framework between loess minerals and acid-neutral and neutral-alkaline water. The values of log
346 K are at 25 °C.

	Mineral-water reaction	log k
	A - Acid (pH<7)	
1	Andesine $Na_{0.6}Ca_{0.4}Al_{1.4}Si_{2.6}O_8(s) + 5.2H_2O + 2.8H^+ = 0.6Na^+ + 0.4Ca^{2+} + 1.4Al(OH)_2^+ + 2.6H_4SiO_4$	-1.34
2	K-feldspar $KAlSi_3O_8(s) + 6H_2O + 2H^+ = K^+ + Al(OH)_2^+ + 3H_4SiO_4$	-7.97
3	Illite $K_{0.6}Mg_{0.25}Al_{2.3}Si_{3.5}O_{10}(OH)_2(s) + 6.6H_2O + 3.4H^+ = 0.6K^+ + 0.25Mg^{2+} + 2.3Al(OH)_2^+ + 3.5H_4SiO_4$	-11.4
4	Clinoenstatite $MgSiO_3(s) + H_2O + 2H^+ = Mg^{2+} + H_4SiO_4$	11.3
5	Glass $Na_{1.3}K_{0.8}Mg_{0.4}Ca_{0.4}Fe(III)_{0.3}Al_{2.6}Si_{11.5}O_{29.2}(s) + 6.6H^+ + 22.6H_2O = 1.3Na^+ + 0.8K^+ + 0.4Mg^{2+} + 0.4Ca^{2+} + 2.6Al(OH)_2^+ + 11.5H_4SiO_4 + 0.3\ Fe(OH)_2^+$	60
6	Chalcedony $H_4SiO_4 = SiO_2(s) + H_2O$	3.55
7	$CO_2(g) + H_2O = H_2CO_3$	-1.5
	B - Basic (pH>7)	
8	Andesine $Na_{0.6}Ca_{0.4}Al_{1.4}Si_{2.6}O_8(s) + 8H_2O = 0.6Na^+ + 0.4Ca^{2+} + 1.4Al(OH)_4^- + 2.6H_4SiO_4$	-19
9	K-feldspar $KAlSi_3O_8(s) + 8H_2O = K^+ + Al(OH)_4^- + 3H_4SiO_4$	-20.6
10	Illite $K_{0.6}Mg_{0.25}Al_{2.3}Si_{3.5}O_{10}(OH)_2(s) + 11.2H_2O = 0.6K^+ + 0.25Mg^{2+} + 2.3Al(OH)_4^- + 3.5H_4SiO_4 + 1.2H^+$	-40.3
11	Clinoenstatite $MgSiO_3(s) + H_2O + 2H^+ = Mg^{2+} + H_4SiO_4$	11.3
12	Glass $Na_{1.3}K_{0.8}Mg_{0.4}Ca_{0.4}Fe(III)_{0.3}Al_{2.6}Si_{11.5}O_{29.2}(s) + 1.4H^+ + 27.8H_2O = 1.3Na^+ + 0.8K^+ + 0.4Mg^{2+} + 0.4Ca^{2+} + 2.6Al(OH)_4^- + 11.5H_4SiO_4 + 0.3\ Fe(OH)_2^+$	34.8
13	Chalcedony $H_4SiO_4 = SiO_2(s) + H_2O$	3.55
14	Calcite $Ca^{2+} + HCO_3^- = CaCO_3(s) + H^+$	-1.85
15	Ca-Montmorillonite $0.165Ca^{2+} + 2.33Al(OH)_4^- + 3.67H_4SiO_4 + 2H^+ = Ca_{0.165}Al_{2.33}Si_{3.67}O_{10}(OH)_2(s) + 12H_2O$	45
16	Montmorillonite-BelleFourche $0.09Na^+ + 0.09K^+ + 0.29Mg^{+2} + 0.24Fe^{+3} + 1.57Al(OH)_4^- + 3.9H_4SiO_4 + 0.09H^+ = (HNaK)_{0.09}Mg_{0.29}Fe_{0.24}Al_{1.57}Si_{3.93}O_{10}(OH)_2 + 910H_2O$	34.9
17	$CO_2(g) + H_2O = HCO_3^- + H+$	-7.8

347

348

3.5.2. Cation exchange coefficients

The cation exchange coefficients distribute the different cations between the water and the exchange complex. Although the value of these coefficients for clays are reported in the literature (Appelo and Postma, 2005), no data are known for loess glass to the authors' knowledge. Cation extraction experiments from volcanic glass with acid solutions revealed that not all the cations exchange in the same way. Contrary to clays, the Na extracted preferentially compared with alkali-earth cations, such as Ca and Mg, which remained in the solid phase (Paul, 1977). A first approximation the cation exchange coefficients between loess/sediment and water in the Chaco-Pampean Plain can be obtained from the unique available data from both the exchange complex composition and the coexisting water. As already said, data consisted on 15 samples of loess sediments and groundwater samples from the Del Azul Creek Basin (Zabala et al., 2016, Table S4).

The exchange equilibrium constants $K_{Na/M}$ represented the NaX following the Gaines-Thomas convention (Appelo and Postma, 2005) (Equations 2 and 3).

$$nNaX + M^{n+} = MX_n + nNa^{+} \quad (2)$$

$$K_{Na/M} = \frac{\beta_{MX_n} a_{Na^+}^n}{\beta_{NaX}^n a_{M^{n+}}} \quad (3)$$

where β is the equivalent fractions and a is the activity of the aqueous ion calculated according to the PHREEQC-Wate4f thermodynamic setting.

First, the average exchangeable base concentrations were converted from meq 100 g^{-1} into eq · kgw^{-1} using a loess porosity of 0.45 and an average solid density of 2.6 g cm^{-3}. The equivalent fractions (β_i) were computed dividing each exchangeable cation concentration by the total CEC. The $K_{Na/M}$ values obtained from Equation 3 are listed in Table 6. As shown in the table, these constants are very different from those for clayey soils. Acccording to the $K_{Na/M}$ values, the

exchange complex of glass shows a tendency to retain K, Ca and Mg, releasing Na to the water. Therefore, a Ca-Mg-K-rich exchange complex is assumed to coexist with Na-rich water.

Table 6. (1) Exchange constants (Eq. 2) calculated for loess glass assuming equilibrium between loess and groundwater from Del Azul Creek Basin data (from Zabala et al, 2016); integrated median from 15 soil samples. (2) Exchange constants for a clayey soil from Appelo and Postma (2005, Table 6.4).

	$K_{Na/K}$	$K_{Na/CaX2}$	$K_{Na/MgX2}$
Loess (glass)(1)	21.4 ± 17	12.8 ± 7	8.9 ± 7
Clayey soil (2)	0.15 to 0.25	0.3 to 0.6	0.4 to 0.6

3.5.3. Mineral dissolution rates

A semi-empirical function was used to describe the kinetics of mineral dissolution (Equation 4). The function is based on the transition state theory and the parameters are determined through laboratory experiments (Lasaga, 1984).

$$r = A\ (k_a a_H^{n_H} e^{-\frac{E_{acid}}{R}(\frac{1}{T}-\frac{1}{298.15})} + k_n e^{-\frac{E_{neutral}}{R}(\frac{1}{T}-\frac{1}{298.15})} + k_b a_H^{n_{OH}} e^{-\frac{E_{basic}}{R}(\frac{1}{T}-\frac{1}{298.15})})\ (\Omega - 1) \quad (4)$$

where r is the dissolution rate (mol kgw^{-1} s^{-1}); A is the reactive surface area (m^2 kgw^{-1}); E is the activation energy (kJ mol^{-1}); k_a, k_m and k_b are the rate constants at acid, neutral and basic pH ranges at 298.15 K (mol m^2 s^{-1}); n is the reaction order of the experiment; a is the activity, and Ω is the mineral saturation (Q/K), where Q is the ion activity product, and K is the equilibrium constant of the mineral. Table 7 compiles the experimental values of k, E and n for the different minerals, which were obtained from the compilation made by Palandri and Kharaka (2004). In the absence of experimental data, the parameters for illite were assumed to be equal to those of muscovite. An estimated glass dissolution rate of 10^{-12} mol m^2 s^{-1} was used given the chemical similarities of the volcanic glass and the most representative primary aluminosilicate minerals of the loess sediments: andesine ($10^{-11.47}$ mol m^2 s^{-1}) and K-feldspar ($10^{-12.41}$ mol m^2 s^{-1}). This intermediate glass dissolution rate is in agreement with recent flow-thought dissolution experiments of several Argentinian volcanic glass samples (Cacciabue et al., 2019).

393 Table 7. Dissolution rates at 25 ºC (log K, mol m^{-2} s^{-1}), experimental dependence on pH (n), and activation energies (E,
394 kJ mol^{-1}) of the solid phases involved in the calculations according to Eq. 4 (from Palandri and Kharaka, 2004).

	$\log k_a$	n_H	E_a	$\log k_n$	E_n	$\log k_b$	n_{OH}	E_b
enstatite	-9.2	0.6		-12.72	80			80
glass	-8.88	0.54	53.5	-12	57.4	-15.6	-0.57	71
andesine	-8.88	0.54	53.5	-11.47	57.4	-15.6	-0.57	71
calcite	-0.3	1	14.4	-5.81	23.5	-3.48	1	35.4
goethite				-7.94	86.5			
K-feldspar	-10.6	0.5	51.7	-12.41	38	-21.2	-0.83	94.1
illite (muscovite)	-11.85	0.37	22	-13.55	22	-14.55	-0.22	22
montmorillonite	-12.71	0.22	48	-14.41	48	-14.41	-0.4	58.9
quartz				-13.4	90.9			

395

396 ### 3.5.4. Mineral precipitation

397 Owing to the limited availability of precipitation rate data, the most straightforward option
398 would be to use the dissolution rate to approximate the precipitation rate. However, this
399 approximation does not take into account the degree of supersaturation required for
400 precipitation to occur, and does not distinguish between homogeneous and heterogeneous
401 nucleation conditions (Lebrón and Suárez, 1996; Nordeng and Sibley, 1994; Steefel and Van
402 Cappellen, 1990). Moreover, it is not easy to determine the precipitation rate because
403 experiments yield metastable products. To overcome these uncertainties, rather than kinetics,
404 the equilibrium assumption was used to calculate the amount of dissolved mineral (calcite,
405 montmorillonite, chalcedony and goethite). Equilibrium constants from Wateq4f data base were
406 used f or that purpose (Ball and Nordstrom, 1991).

407 ### 3.5.5. The S·t lumped parameter

408 The amount of solute transferred between the solid and water phases depends on the mineral
409 reaction rates and on the time of reaction. The mineral reaction rates can be calculated
410 according to Equation 4. Most of the parameters involved in this equation are known from
411 laboratory experiments and thermodynamic calculations. The reactive surface area S, however,
412 is difficult to determine. In laboratory experiments it is currently measured by gas sorption (BET)
413 experiments. In a porous medium, it could be estimated from the grain size, assuming that grains
414 are spheres. Thus (see section 2.4.1), a grain surface area of 100 m^2 kgw^{-1} was estimated for a

coarse silt grain size of 31 μm and a porosity of 0.45. However, water usually circulates along preferential paths and the actual mineral surface area in contact with water is very difficult to assess. For instance, if groundwater circulates in a set of fractures separated 1 mm, the final wetted surface would be 2.5 m^2 kgw^{-1}. In fact, mineral dissolution rates measured in the field can show values significantly lower than those measured in the laboratory (White and Brantley, 1995). As regards the time of reaction, although maximum ages of 50 years have been determined from ^3H studies (section 2.2), the exact time t of mineral-water reaction in each particular case is also uncertain. Since parameters S and t contain uncertainties and since they are always terms of a product in the calculations, they cannot be discussed independently and, therefore, a single lumped parameter S·t (m^2 kgw^{-1} yr) has been used. Thus, a value of 100 m^2 kgw^{-1} yr can result from a reactive surface area of 100 m^2 kgw^{-1} (silt) and a reaction time of 1 year, or from a surface area of 2.5 m^2 kgw^{-1} (fractures) and 50 year.

4. Results and discussion

4.1. Groundwater chemistry: analytical values

The chemical composition of groundwater samples and saturation indices (SI) of the minerals for the three regions considered are listed in Table 8, Table S5 and Table S6, and the main results are ploted with respect to pH in Figure 3. In terms of dissolved solutes, the Na concentration in groundwater increases with pH, whereas Ca and Mg show a downwards trend (Figure 3a, b, c). The K and Si concentrations remain more or less stable at any pH (Figure 3d, e). Alkalinity (quoted as HCO_3) underwears the same evolution as Na, increasing slightly with pH (Figure 3f). Consistently with observations in other localities of the CPP, As concentration clearly increases with pH and HCO_3 (Figure 4), and the samples with pH higher than 8 contain As above 10 μg/L, the WHO recommended value (Figure 3g). Only one sample of the NLP has As concentration below the detection limit (4 μg L^{-1}) (Table S5). No As correlation with Si was observed in the analyses of the samples from the three localities studied, whereas other anions increasing As

mobility such as P, V or Mo were not detected in general. The dispersion of Cl was attributed to the evapoconcentration process, resulting in a higher Cl concentration in the arid NLP and lower values in the more humid MRAS (Figure 3h).

Table 8. Measured chemical composition of groundwater samples from the Matanza-Riachuelo Aquifer System. Units in mg L^{-1}, except for Al and As (µg L^{-1}).

Matanza-Riachuelo Aquifer System in Buenos Aires Province (MRAS)												
ID	Prof. (m)	pH	T (^{o}C)	Ca	Mg	Na	K	HCO_3	Cl	Si	Al	As
18F	13.6	7.4	20	77	27	110	9.5	460	36	13	30	31.6
7F	15.7	7.7	20	48	19	96	20	300	32	43	110	29
24F	14.6	7.4	20	64	27	150	12	460	68	32	-	21
15F	17.2	7.5	23	54	19	160	9.3	490	65	4.5	670	31.4
2F	13.3	7.6	22	46	19	160	30	450	29	30	30	54.6
22F	14.3	7.7	19	39	13	150	15	430	64	5.5	75	26.8
12F	14.2	7.5	19	72	26	270	16	510	96	99	2400	36.8
23F	14.5	7.4	20	49	23	190	13	550	57	8.4	88	40.3
32F	15	7.7	18	39	13	160	6.2	390	65	20	260	48.8
11F	14.2	7.4	19	67	32	390	27	970	36	17	30	28.3
36F	19.8	7.8	21	28	8.3	170	8.9	410	63	9.9	1400	57.9
25F	15.7	8.0	19	23	6	160	9.4	360	73	7.4	1200	104
17F	14.9	7.7	19	30	15	210	15	520	89	6	30	83.6
19F	13.3	7.8	18	40	8.6	330	17	760	37	22	30	92.7
27F	17	7.8	21	19	14	220	12	470	56	24	30	25.5
20F	14	8.0	18	23	13	290	11	620	59	9.9	100	182
30F	14.8	8.0	19	17	12	260	15	580	93	9.9	-	109
35F	18.9	7.8	20	21	9.7	360	12	660	53	42	1600	0

All the loess aluminosilicates (andesine, K-feldspar, illite, montmorillonite) showed an increasing SI from acid (pH = 6.67) to neutral-alkaline pH values (pH≈8). However, at higher pH values (pH>8) the aluminosilicates SI decreased, reaching equilibrium and even in some cases subsaturation (Figure 3i, k, l, m). The SI of glass was only computed for the RDA (SI = -78.9 to -84.7) with the Fe analytical data, whereas in MRAS and NLP Fe concentration was assumed to be the instrumental detection limit (5 µg L^{-1}). Glass is maintained clearly subsaturated for all pH values in all the regions. In contrast to aluminosilicates, clinoenstatite SI increased regularly with pH without reaching equilibrium (Figure 3n). Calcite also showed an increase in SI at low pH and

454 reached equilibrium at neutral pH (Figure 3j). As expected, the CO_2 pressure decreased with

455 increasing pH (Figure 3o).

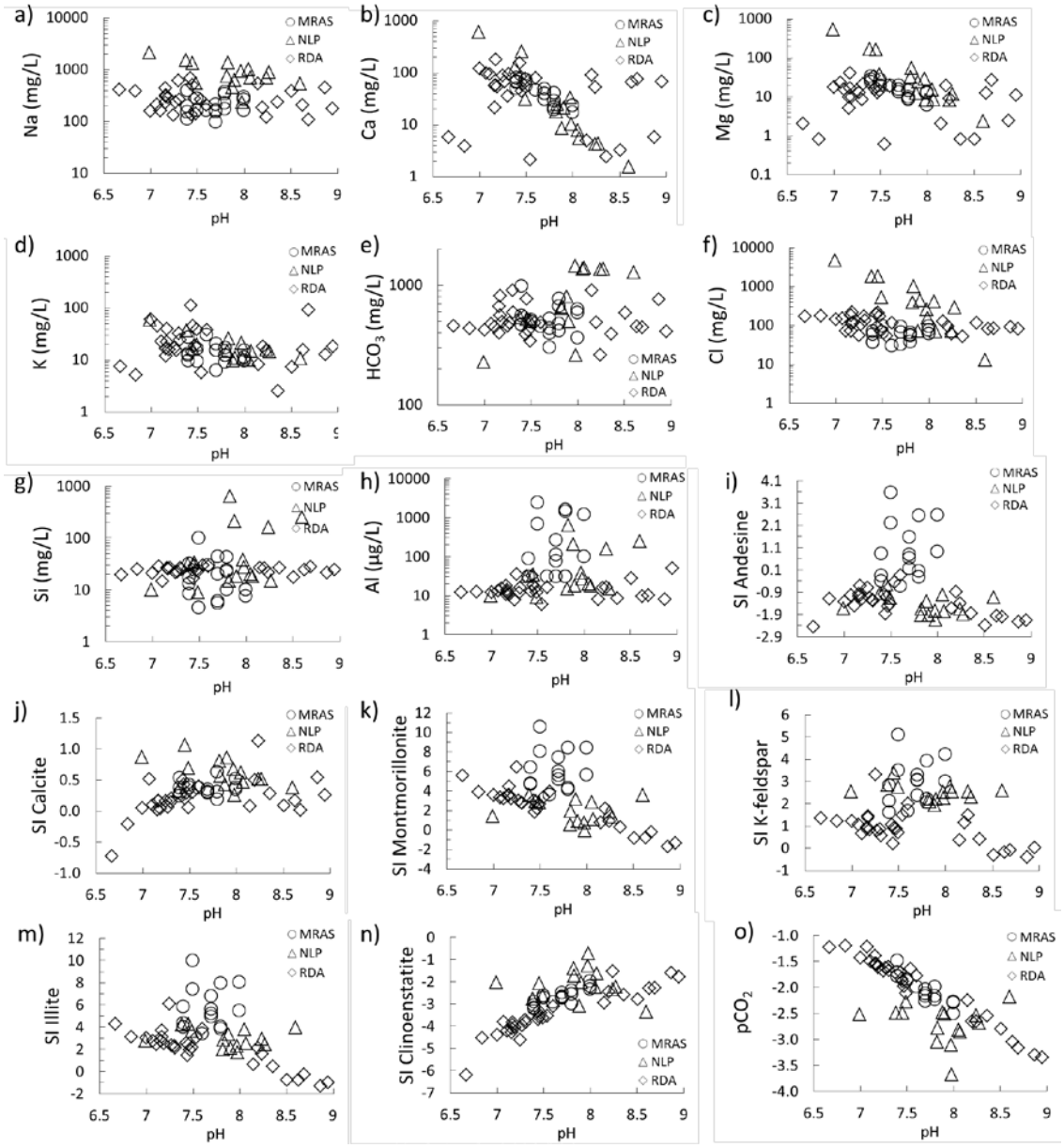

456

457 Figure 3. Concentration of the major cations, anions and mineral saturation indices (SI) in groundwater versus pH.
458 (O): Matanza-Riachuelo Aquifer System (MRAS); (Δ): Northern of the La Pampa province (NLP) (Smedley et al. (2002);
459 (◊): Río Dulce Alluvial Aquifer (DRA) (Sifuentes and Nordberg, 2003). Glass saturation was only able to be calculated
460 for the RDA region as no Fe measurements were available for the MRAS and NLP regions.

461

462 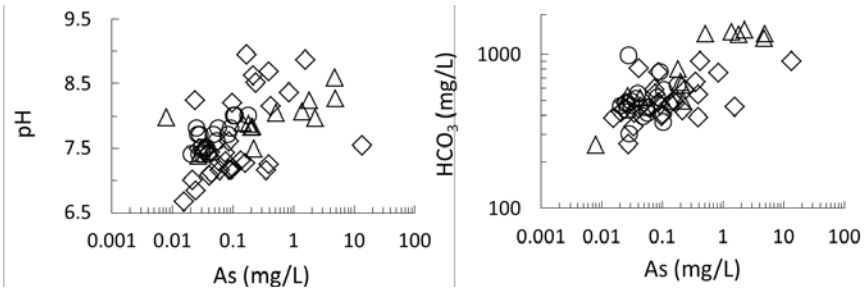

463 Figure 4. Variation of total As concentrations with pH and HCO_3 in the three modeled areas: (Δ) a Northern of La
464 Pampa province (NLP) (Smedley et al., 2002); (◊) the Río Dulce Alluvial Aquifer (DRA) (Sifuentes and Nordberg, 2003)
465 and (O) the Matanza-Riachuelo Acuifer System (MRAS) (this study).

466 The exchange complex revealed predominance of CaX_2 and to a lesser extent MgX_2 although
467 only data from MRAS were available (see Table 3). In summary, the CPP groundwater chemistry
468 showed an increase in Na and in alkalinity and a decrease in Ca and Mg with pH. The illite, K-
469 feldspar and montmorillonite were supersaturated reaching equilibrium at high pH (pH>8);
470 andesine, glass and clinoenstatie were subsaturated, whereas calcite was in equilibrium in most
471 cases.

472 4.2. Calculated groundwater chemistry: the base case

473 The evolution of the major solutes, pH and the exchange complex of the three models are
474 plotted in Figure 5. The measured data ranging between the first and the third quartiles (Q1,
475 25%; Q3, 75%) are also plotted for comparison. As explained in section 3.5.5, a value of 40 m^2
476 kgw^{-1} yr^{-1} for the abscissa can result either from a reactive surface area of 100 m^2 kgw^{-1} (coarse
477 silt, 31 µm) and a reaction time of 5 months, or from a reactive surface area of 200 m^2 kgw^{-1}
478 (medium silt, 15 µm) and a reaction time of 2.5 months. Therefore, the X-axis can be read as the
479 time evolution for a fixed loess particle size. As stated abovem, this S·t value is highly uncertain
480 and a sensistivity analysis will be discussed below (section 4.3.1).
481 A sharp increase of solute concentrations occurred when the input of acid rainwater (pH= 5.6),
482 subsaturated in all primary silicates, entered into contact with the loess silicates. The
483 geochemical reaction framework between the input rainwater and the loess minerals consumed
484 protons and released Na, Ca, K and Mg to the aqueous phase owing to andesine, glass, K-

485 feldspar, clinosentatite and illite dissolution (Table 5A). After the first water-loess contact
486 neutrality was achieved, and reactions changed to that of Table 5B. In agreement with the
487 measured SI values, at this stage only andesine, glass and clinoenstatite remained subsaturated,
488 releasing Na, Ca, Mg and K into the solution. The continuous release of Na resulted in the
489 concentration of the CPP groundwater. The evolution of Ca was affected by montmorillonite
490 and calcite precipitation, and the evolution of Mg and K by the cation exchange retention. Owing
491 to the low amount of montmorillonite precipitated with respect to volcanic glass, the total CEC
492 value was considered constant (and due to glass) during the calculation.

493 As regards to anion concentrations, alkalinity increased by one order of magnitude because of
494 edaphic CO_2 dissolution due to the pH increase. The Cl concentration was maintained constant.
495 Finally, the Si concentration was probably constrained by chalcedony precipitation.

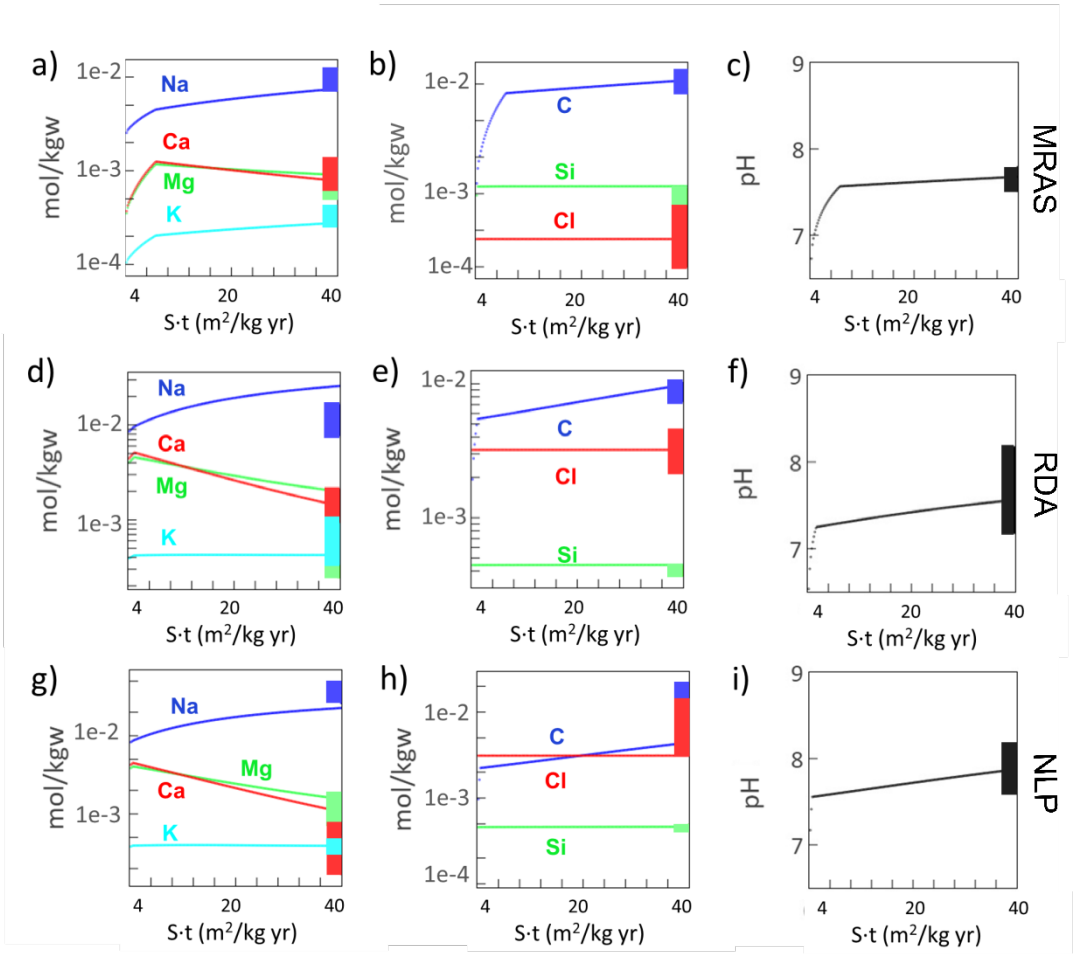

496

497 Figure 5. Modelled evolution (lines) of the major cations, anions and pH in soil water of the Chaco-Pampean Plain. a,
498 b, c) Matanza-Riachuelo Aquifer System. d, e, f) Río Dulce Alluvial Aquifer. g, h, i) Northern of the La Pampa province.
499 Measured values (Q1 – Q3 range) are represented by vertical bars.

500 Comparison of the three regions shows that the best results were obtained for the MRAS
501 predictions, where solutes and pH fell within the Q1-Q3 range of the measured groundwater
502 samples. Although some solutes from the RDA and NLP models do not fall within the measured
503 Q1-Q3 range, they are within the maximum and minimum values. This could be due to a lack of
504 representativity of the input rainwater used, as due to the absence of rainwater samples of each
505 of the three regions, the MRAS rainwater chemistry was extrapolated to the entire CPP, thus
506 favoring the MRAS prediction. The rainwater chemistry in the NLP region is expected to be
507 enriched in Cl and Na due to the incorporation of salt particles from the atmospheric dust.
508 Raychowdhury et al. (2014) modelled the NLP groundwater chemistry and noticed the
509 importance of the evapoconcentration process and/or the salinas salt incorporation. In the NLP,

during the dry season evaporation resulted in salt incrustations visible along the lake shores (Smedley et al., 2002), and the strong winds in the region favor this salt to enrich the atmospheric dust. These salts are dissolved during rainfall, producing high Cl concentrations in the shallowest part of the aquifer. There is evidence for this process in the similar concentrations of Na and Cl in groundwater from NLP (Figure 5), which results in an overestimation of the evapoconcentration factor. This leads to an increase in the initial mineral SI and a subsequent delay of the silicate dissolution rates, and therefore in the Na and C concentrations. Carbon concentrations and speciation are also affected by the CO_2 pressure and its role is discussed below.

4.3. Sensitivity analysis

The sensitivity analysis seeks to shed light on the processes driving the groundwater to high pH (pH>8) and alkalinity values, and resulting in elevated As concentrations. To this end, the unconstrained parameters CO_2 pressure and rock surface area lumped with time (S·t) were established between two extreme values.

4.3.1. The role of the S·t parameter and of the soil CO_2 pressure

The impact of the reactive surface area on pH and alkalinity was studied by varying the S·t parameter from 0 to 400 $m^2\ kg^{-1}\ yr^{-1}$. Here, 0 $m^2\ kg^{-1}\ yr^{-1}$ signifies the absence of silicate weathering and 400 $m^2\ kg^{-1}\ yr^{-1}$ accounts for very fine loess particles (4·µm) that react for one year. Likewise, 400 $m^2\ kg^{-1}\ yr^{-1}$ could be achieved when coarse silt (31 µm) reacts for 4 years or when fine sand particles (200 µm) react for 10 years. At the same time, the role of the CO_2 pressure was evaluated by increasing the value from $10^{-3.5}$ to 10^{-1} bar. The former represents the atmospheric value and the latter a very intensive root respiraton and microbiological soil activity (Witkamp, 1966; Kucera and Kirkham, 1971).

Figure 6 shows the calculated pH and alkalinity (quoted as C concentration) after using different S·t and soil CO_2 pressures (quoted as pCO_2). Both the measured alkalinity in groundwater and the predicted pH>8 areas, critical for As concentrations, are depicted by dashed lines (Figure 6c, f, i). The highest pH values (pH>8.5) modelled are also indicated, although they were only measured in the DRA region. The intersection of dashed lines shows the most probable range of S·t and pCO_2 values to account for the observed groundwater composition. The areas depicted comprise S·t values from 40 to 200 m^2 kg^{-1} yr^{-1}, slightly narrower for NLP. The observations can be explained with a wide range of reasonable parameters, from a coarse to fine silt grain size (31 to 8 µm) reacting during one year, to a fine sand (200 to 370 µm) reacting during 50 yr. On the other hand, the CO_2 pressures required to model the observed pH and alkalinity values range from 10^{-2} to $10^{-3.5}$ bar.

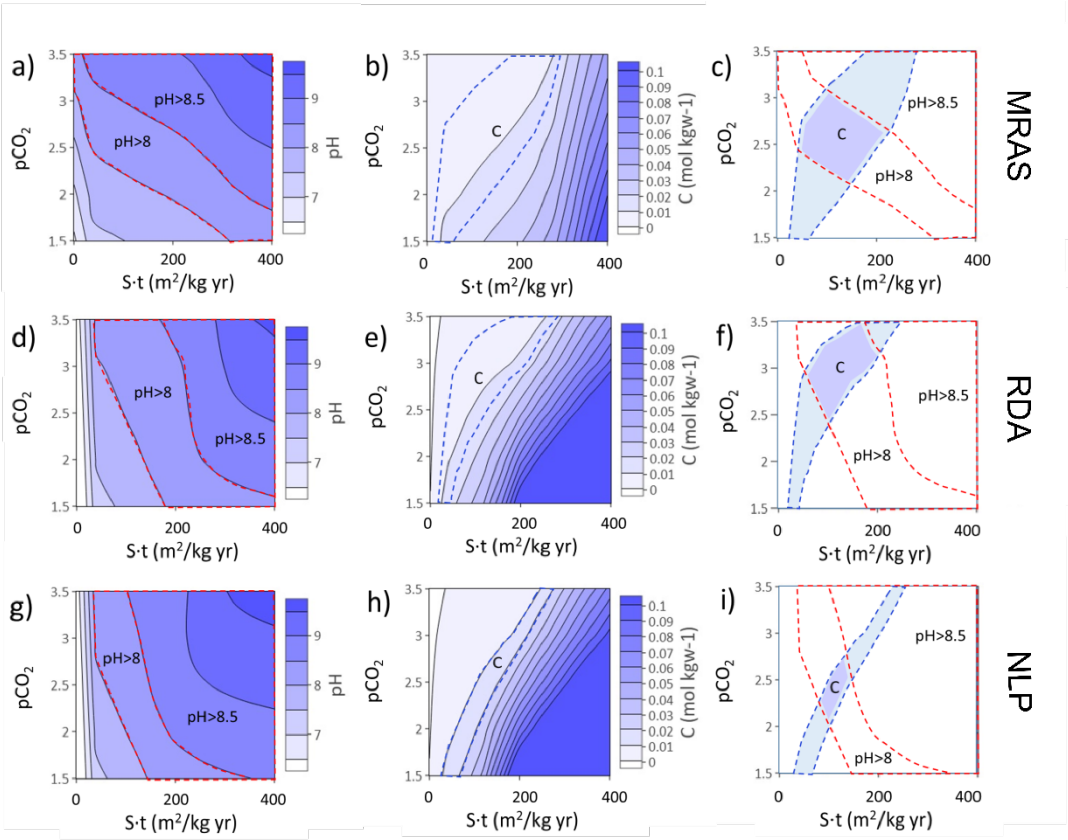

Figure 6. Evolution of pH and alkalinity in terms of dissolved C (mol kgw^{-1}) using different values for the lumped parameter reactive rock surface areas and reaction times (S·t) and CO_2 pressure (as pCO_2). a, b, c) Matanza-Riachuelo Aquifer System. d, e, f) Río Dulce Alluvial Aquifer. g, h, i) Northern of the La Pampa province. The fields of pH>8 and the measured alcalinities are depicted. The intersection of dashed lines in c), f), d) shows the most probable range of S·t and pCO_2 values to account for the observed groundwater composition.

According to Figure 6, pH and alkalinity increase with decreasing CO_2 pressure, decreasing grain size and/or increasing reaction time. Even if the three factors are crucial, low CO_2 pressures (< $10^{-2.5}$ bar) are necessary in order to reach the higher pH values (pH>8.5) related to the higher As concentrations in groundwater. Low CO_2 pressures are associated with poorly vegetated soils.

4.3.2. The role of cation exchange and secondary minerals precipitation

Earlier loess mineralogical studies have confirmed the existence of secondary calcite and montmorillonite as well as an important exchange capacity for loess (Teruggi, 1957; González Bonorino, 1965; Zinck and Sayago, 1999; Martínez and Bocanegra, 2002; Bonorino et al., 2005; Tófalo et al., 2005; Aullón, 2013, Zabala et al., 2016). This section deals with the role of cation exchange reactions and the secondary precipitation of calcite and montmorillonite in the chemical composition of groundwater. Our analysis is focused on pH and alkalinity, the main factors of As mobility.

4.3.2.1. The role of calcite precipitation

As the average calcite saturation index of the measured samples ranged between 0.2 and 0.3, calcite was considered to be in equilibrium in all the earlier calculations. A simulation without calcite precipitation was performed to evaluate the relevance of this process for groundwater chemical composition. The resulting pH and alkalinity in terms of S·t and CO_2 pressure are plotted in Figure 8.

At acid pH, most of the silicate reactions consume acidity thus increasing the pH (Table 5A). At basic pH, clinoenstatite and glass remain undersaturated (Figure 3) and still dissolve, consuming acidity (Table 5B, Eq. 11 and 12) and promoting the dissolution of CO_2 (Table 5B, Eq. 17). Calcite precipitation is the main process consuming alkalinity and consequently controlling the increase of pH and alkalinity (Table 5B, Eq.14). In the absence of calcite precipitation, alkalinity and pH

increase rapidly, exceeding the measured groundwater values (Figure 7). Thus, the pH and alkalinity measured values could only be attained at less than 50 m^2 kg^{-1} yr^{-1}, i.e., assuming that loess particles were medium to coarse sand, and/or fast reaction time. These results are not realistic for loess, and moreover the S·t values required to fulfill the measured alkalinity and pH values do not coincide. Therefore, calcite precipitation plays a key role in preventing extremely high alkaline groundwaters.

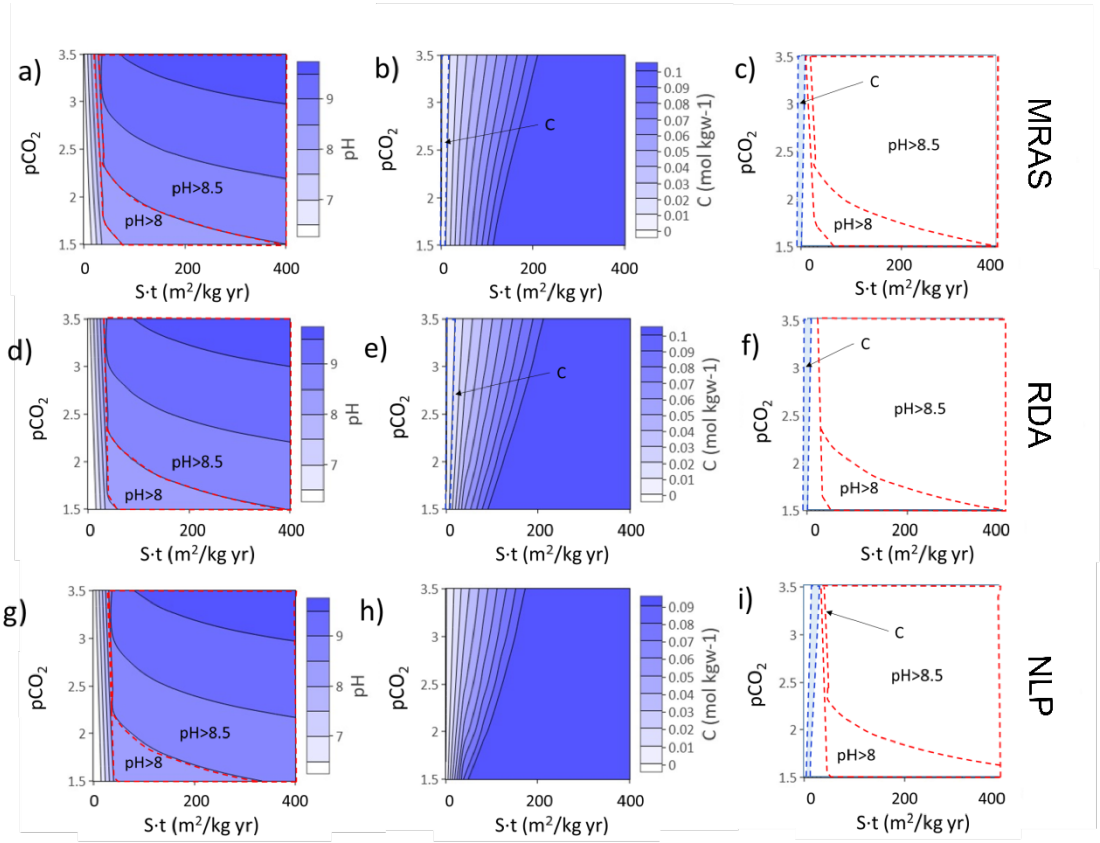

Figure 7. Evolution of pH and alkalinity (as C, mol kgw^{-1}) using different lumped reactive surface area and time (S·t*)* and CO_2 pressure (as pCO_2) without calcite precipitation. a, b, c) Matanza-Riachuelo Aquifer System. d, e, f) Río Dulce Alluvial Aquifer. g, h, i) Northern of the La Pampa province. The fields of pH>8 and the measured alcalinities are depicted. The intersection of dashed lines in c), f), d) shows the most probable range of S·t and pCO_2 values to account for the observed groundwater composition.

4.3.2.2. The role of cation exchange

A simulation was performed without cation exchange processes. Apart from andesine dissolution, the release of CaX_2 from the exchanger to the solution is the main Ca source for

590 calcite precipitation. Without this Ca contribution from the exchange complex, calcite
591 precipitation decreased dramatically between ten and three times in the three localities studied.
592 Since the results are identical to those reported for the absence of calcite in section 4.3.2.1, they
593 are not plotted. Therefore, even if the cation exchange process seems to have a minor role in
594 the groundwater chemistry, it is critical to maintain the precipitation calcite. Thus, cation
595 exchange is also capital to reach the alkalinity and pH values measured in groundwater of the
596 Chaco-Pampean Plain.

597 #### 4.3.2.3. The role of secondaty clay formation

598 According to their positive saturation index in all the groundwater samples (average of 5.8, 2.9
599 and 2.3 for MRAS, RDA and NLP, respectively), montmorillonite precipitated in all the previous
600 models. In order to determine its impact in the final composition of groundwater, a new
601 modeling was performed inhibiting the precipitation of montmorillonite. The results are plotted
602 in Figure 8.

603 Montmorillonite precipitation at pH>7 consumes protons because of Al aqueous speciation
604 (Table 5B, Eq. 15). Thus, should montmorillonite fail to form, unrealistic low values of pH would
605 result. In the MRAS case, the measured pH values close to 8 would only be possible at CO_2
606 pressures close to the atmospheric value (Figure 8a), whereas the alkalinity values recorded in
607 groundwater would only exist at CO_2 pressures higher than 10^{-2} bar (Figure 8b). The predicted
608 pH and alkalinity values for RDA and NLP were even more unrealistic where pH>8 were not
609 attained (Figure 8d, g). Measured groundwater alkalinity in RDA only existed at CO_2 pressures
610 exceeding 10^{-2} bar (Figure 8e), whereas the measured alkalinity values in NLP were not reached
611 (Figure 8h). Montmorillonite formation, therefore, is essential for groundwater to achieve the
612 measured pH and alkalinity.

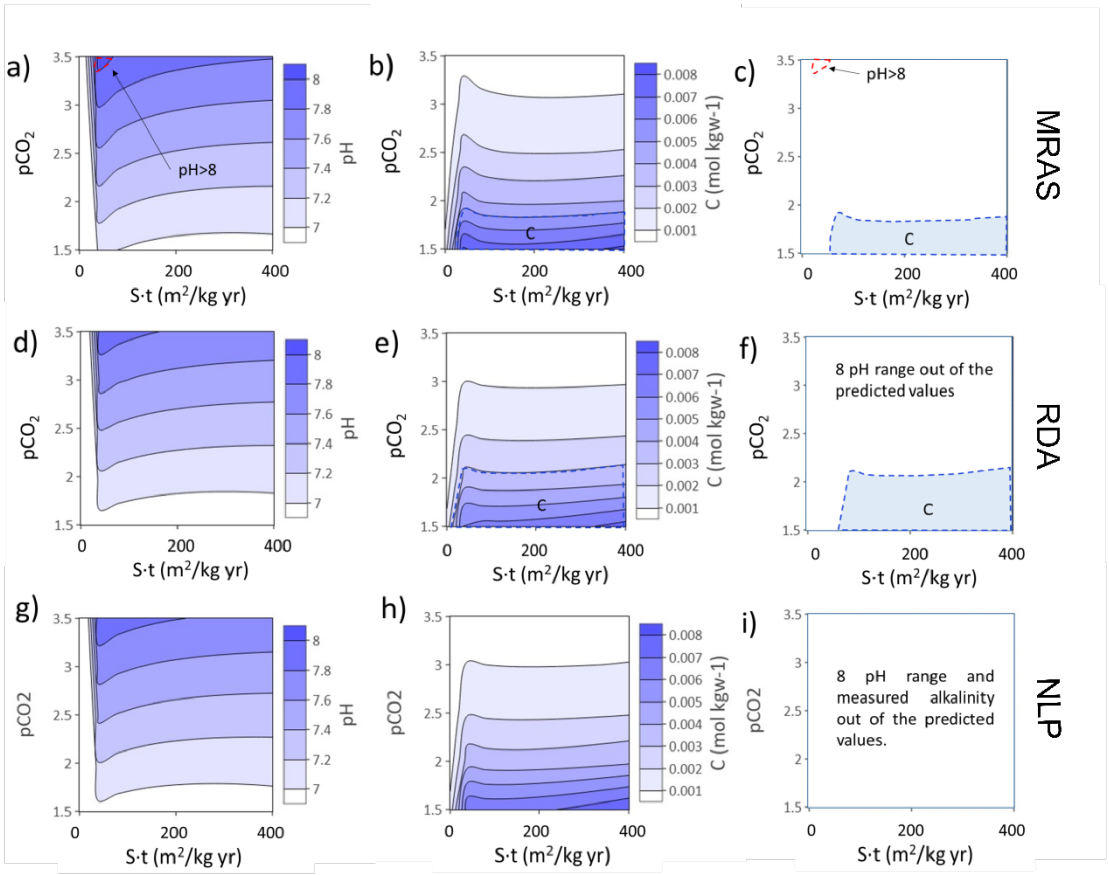

Figure 8. Evolution of pH and alkalinity (as C, mol kgw^{-1}) using different lumped reactive surface area and time (S·t) and CO_2 pressure (as pCO_2) after one-year or water rock reaction without montmorillonite precipitation. a, b, c) the Matanza-Riachuelo Aquifer System (MRAS); d, e, f) Río Dulce Alluvial Aquifer (DRA); g, h, i) Northern area of the La Pampa province (NLP). The fields of pH>8 and the measured alcalinities are depicted. The intersection of dashed lines in c), f), d) shows the most probable range of S·t and pCO_2 values to account for the observed groundwater composition.

In earlier calculations, montmorillonite of Ca-rich composition was assumed as proxy for secondary clays. However, no mineralogical analyses recording the actual Chaco-Pampean montmorillonite compositions were available. Then, secondary clays may also contain other cations such as Mg, K and Na, as these ions are also released by primary silicate dissolution. Thus, the impact of the clay composition on the groundwater chemistry was also analyzed by using the well determined Belle Fourche, South Dakota, montmorillonite $[(HNaK)_{0.09}Mg_{0.29}Fe_{0.24}Al_{1.57}Si_{3.93}O_{10}(OH)_2]$ (Kittrick, 1971).

The chemical stability of montmorillonite depends on its ion composition. The difference between the Ca-Montmorillonite and the BelleFourche-Montmoillonite equilibrium constants (Table 5, Eq. 15 and Eq. 16) led to a marked decrease in the precipitated montmorillonite.

Consequently, in the use of the BelleFourche-montmorillonite also yielded in low unrealistic low pH and alkalinity values. The chemical composition and thermodynamics of the actual clay minerals from the Chaco Pampean Plain is probably similar to that proposed for Ca-montmorillonite. Further investigation on this point is still needed, because secondary clay formation is indispensable for increasing the pH and alkalinity and especially for attaining the highest values.

5. Conclusions

The analyses of groundwater from three different regions (from humid to arid) in the Chaco-Pampean Plain confirm the positive correlation between arsenic and the high pH and HCO_3 concentrations. Thus, the groundwater samples from the three regions with pH values exceeding 8 are more prone to contain As concentrations above 0.01 mg L^{-1}, the limit recommended by the WHO. A geochemical model describing the loess-water interactions occurring in the soils enabled us to gain further insight into the origin of high pH, Na-HCO_3 water type and arsenic mobility in groundwater.

Comparison of predicted and observed values of pH and alkalinity allowed us to select the CO_2 pressure (from 10^{-2} to $10^{-3.5}$ bar) and the S·t (of 80 to 200 m^2 kg^{-1} yr^{-1}) to obtain the observed pH>8 and alkalinity values essential for As mobility. Furthermore, very low CO_2 pressures ($<10^{-3}$ bar) characteristic of poorly vegetated soils and arid areas are crucial for attaining the highest measured pH values (pH>8.5). In coherence with this result, the highest As concentrations are recorded in the NLP region. The interpretation of the S·t range is less conclusive, as the measured groundwater chemistry can be obtained by a wide range of combinations between a reactive surface area of fine silt with one year contact and a reactive area of fine sand with over fifty years contact.

The formation of secondary minerals has a critical impact on the resulting groundwater composition. As expected, calcite precipitation was necessary to maintain the calculated pH and

alkalinity within the measured ranges, preventing unrealistically high alkaline groundwaters. Calcite precipitation has been widely considered in the literature on the CPP. However, this is the first CCP model accounting for a measured (real) CEC. The exchange complex of the volcanic glass has revealed as a very important source of Ca required for calcite precipitation, and therefore to reach the measured pH and alkanity in groundwater. Further investigation on the role of volcanic glass in the soil exchange properties and the chemical composition of the exchange complex is needed to understand the hydrochemistry of groundwater in the Chaco-Pampean Plain.

Significantly, the precipitation of secondary clays (Ca-montmorillonite in this study) was vital to obtain the higher pH and alkalinity values recorded. In addition to its role in pH and alkalinity, the chemistry of the clay exerted a major influence on groundwater composition. Again, the characterization of the clay mineralogy of soils is therefore essential in improving the understanding of the high pH and alkalinity values of groundwater, especially as relates to As mobility.

Acknowledgements

This work has been funded by the Autoridad de Cuenca Matanza Riachuelo (ACUMAR). S.A. The first author thanks the National Council of Scientific and Technical Research (CONICET, Argentina) for doctoral fellowship.

Author Contribution

Armengol, S., Ayora, C, Manzano, M. and Bea, S. A. conceived of the presented idea. Armengol, S. and Manzano, M. performed the measurements. Armengol, S. and Ayora, C. carried out the calculations. Armengol, S and Ayora, C. took the lead in writing the manuscript. Ayora, C.,

Manzano, M. , Bea, S. A., and Martínez, S. helped supervise the project. All authors discussed the results and commented on the manuscript.

References

Appelo, C. A. J., Postma, D. (2005). Geochemistry, groundwater andpollution. Rotterdam, Netherlands, AA Balkema. Segunda Edición.

APHA (2005). Standard methods for the examination of water and wastewater, 21st ed. APHA-AWWA-WEF, Washington, D.C.

Aradóttir, E. S. P., Sigfússon, B., Sonnenthal, E. L., Björnsson, G., Jónsson, H. (2013). Dynamics of basaltic glass dissolution–Capturing microscopic effects in continuum scale models. Geochimica et Cosmochimica Acta, 121, 311-327.

Armengol, S., Manzano, M., Bea, S. A., Martínez, S. (2017). Identifying and quantifying geochemical and mixing processes in the Matanza-Riachuelo Aquifer System, Argentina. Science of the Total Environment, 599, 1417-1432.

Aullón, A. (2013). Distribution and Mobility of Arsenic in the Shallow Aquifers of Northeastern of La Pampa Province, Argentine MSc Thesis, Department of Land and Water Resources Engineering).

Ball, J. W., Nordstrom, D. K. (1991). User's manual for WATEQ4F, with revised thermodynamic data base and test cases for calculating speciation of major, trace, and redox elements in natural waters.

Bhattacharya, P., Claesson, M., Bundschuh, J., Sracek, O., Fagerberg, J., Jacks, G., Thir, J. M. (2006). Distribution and mobility of arsenic in the Río Dulce alluvial aquifers in Santiago del Estero Province, Argentina. Science of the Total Environment, 358 (1-3), 97-120.

Blanco, M. D. C., Paoloni, J. D., Morrás, H. J. M., Fiorentino, C. E., Sequeira, M. (2006). Content and distribution of arsenic in soils, sediments and groundwater environments of the southern Pampa region, Argentina, Environmental Toxicology: An International Journal, 21(6), 561-574.

704 Blanes, P., Herrera Aguad, C., Jiménez, M.C. (2006). Arsénico y otros oligoelementos asociados
705 en aguas subterráneas de la provincia del Chaco: estudio preliminar, Libro de Resúmenes del
706 Taller de Distribución del As en Iberoamérica (ed. Litter, M.), Argentina, 61-62.
707 Blarasin, M. (2003). Geohidrología ambiental del Sur de Córdoba, con énfasis en la ciudad de Río
708 Cuarto y su entorno rural. PhD Dissertation, Universidad Nacional de Río Cuarto,
709 unpublished.
710 Boletta, P. E., Ravelo, A. C., Planchuelo, A. M., Grilli, M. (2006). Assessing deforestation in the
711 Argentine Chaco. Forest Ecology and Management, 228(1-3), 108-114.
712 Bonorino, A. G., Limbozzi, F., Albouy, R., Lexow, C. (2008). Movilidad de metales y otros
713 elementos en el acuífero loéssico regional del suroeste bonaerense, Geoacta, 33, 31-42.
714 Borzi, G. E., Garcia, L., Carol, E. S. (2015). Geochemical processes regulating F−, as and NO3−
715 content in the groundwater of a sector of the Pampean Region, Argentina. Science of the
716 Total Environment, 530, 154-162.
717 Bourcier, G. F., Lowdon, J. (1992). U.S. Patent No. 5,133,505. Washington, DC: U.S. Patent and
718 Trademark Office.
719 Brook, G. A., Folkoff, M. E., Box, E. O. (1983). A world model of soil carbon dioxide. Earth Surface
720 Processes and Landforms, 8(1), 79-88.
721 Bundschuh, J., Farias, B., Martin, R., Storniolo, A., Bhattacharya, P., Cortes, J., Bonorino, G.,
722 Albouy, R. (2004). Groundwater arsenic in the Chaco-Pampean Plain, Argentina: case study
723 from Robles country, Santiago del Estero Province. Applied Geochemistry, 19, 231-243.
724 Cacciabue, L., Ayora, C., Cama, J. (2019). Arsenic release from Agerntinean loess and volcanic
725 ashes. Goldschmidt, Barcelona 18-23 August.
726 Cohen, D., Ward, C. R. (1991). SEDNORM—a program to calculate a normative mineralogy for
727 sedimentary rocks based on chemical analyses. Computers and Geosciences, 17(9), 1235-
728 1253.

729 Dzombak, D.A., Morel, F.M.M. (1990). Surface Complexation Modeling: Hydrous Ferric Oxide.
730 John Wiley and Sons, New York, 416.
731 Farías, S., Casa, V., Vazquez, C., Ferpozzi, L., Pucci, G., Cohen, I. (2003). Natural contamination
732 with arsenic and other trace elements in groundwaters of Argentina Pampa Plain. Science of
733 the Total Environment, 309, 187-99.
734 Fernández-Turiel, J. L., García-Valles, M., Gimeno-Torrente, D., Saavedra-Alonso, J., Martínez-
735 Manent, S. (2005). The hot spring and geyser sinters of El Tatio, Northern Chile. Sedimentary
736 Geology, 180 (3-4), 125-147.
737 Fiorentino, C.E., Paoloni, J.D., Sequeira, M.E., Arosteguy, P. (2007). The presence of vanadium
738 in groundwater of southeastern extreme the pampean region Argentina: relationship with other
739 chemical elements, Journal of Contaminant Hydrology, 93(1-4), 122-129.
740 Gao, X.B., Wang,,Y.X., Hu, Q.H., Su, C.L. (2011) Effects of anion competitive adsorption on
741 arsenic enrichment in groundwater. Journal of Environmental Science and Health Part A-
742 Toxic/hazardous Substances & Environmental Engineering, 46(5), 471-479.García, M. G.,
743 Sracek, O., Fernández, D. S., del Valle Hidalgo, M. (2007). Factors affecting arsenic
744 concentration in groundwaters from Northwestern Chaco-Pampean Plain, Argentina.
745 Environmental Geology, 52(7), 1261-1275.
746 González- Bonorino, F. (1965). Soil clay mineralogy of the Pampa plains. Journal of Sedimentary
747 Petrology, 36, 1026-1035.
748 Gröning, M., Lutz, H. O., Roller-Lutz, Z., Kralik, M., Gourcy, L., Pöltenstein, L. (2012). A simple rain
749 collector preventing water re-evaporation dedicated for $\delta^{18}O$ and $\delta^{2}H$ analysis of cumulative
750 precipitation samples. Journal of Hydrology, 448, 195-200.
751 Guber, R.S., Tefahal, L., Arias, N., Sandoval, N., Toledo, R., Fernandez, M., Cayetano, B., Martínez,
752 M., Soria de González, A. (2009). Contenido de arsénico en el agua de consumo en Leales y
753 Graneros (Prov. de Tucumán, Argentina). Acta Bioquímica Latinoamericana, 2, 1-10.
754 IHLLA (2012). Modelo Conceptual y Numérico del flujo de agua subterránea de la cuenca

del río Matanza-Riachuelo. Instituto de Hidrología de Llanuras (Conceptual and Numerical Model of Groundwater Flow in the Matanza-Riachuelo Basin). Final Report. Developed by the Instituto de Hidrología de Llanuras, Azul, Argentina, for the Autoridad de Cuenca Matanza-Riachuelo, pp. 227.

INTA, 1979. Atlas de Suelos de la República Argentina, Misiones. Centro de Investigaciones de recursos Naturales, Instituto Nacional de tecnología Agropecuaria. Secretaria de Ganadería, Agricultura y Pesca, Buenos Aires, 111–154.

Iriondo, M.H. (1997). Models of deposition of loess and loessoids in the upper Quaternary of South America. Journal of South American Earth Sciences, 10, 71-79.

Johnson J, Anderson F, Parkhurst DL. (2000) Database thermo.com.V8.R6.230, Rev 1.11. Lawrence Livermore National Laboratory, Livermore, California.

Kent, D.B., Niedan, V.W., Isenbeck-Scrötter, M., Stadler, S., Jann, S., Höhn, R., Davies, J.A. (2003). The influence of oxidation, reduction and adsorption reactions on arsenic transport in the oxic, suboxic and anoxic zones of a mildly acidic sand and gravel aquifer; http://wwwbrr.cr.usgs.gov/Arsenic/FinalAbsPDF/kent.pdf (Accessed on February 17, 2003).

Kittrick, J. A. (1971). Stability of Montmorillonites: I. Belle Fourche and Clay Spur Montmorillonites 1. Soil Science Society of America Journal, 35(1), 140-145.

Kucera, C. L. and Kirkham, D. R. (1971). Soil respiration studies in tall grass prairie in Missouri. Ecology, 52, 912-915.

Lasaga, A. C. (1984). Chemical kinetics of water-rock interactions. Journal of Geophysical Research-Solid Earth, 89(B6), 4009-4025.

Lebrón, I. and Suárez, D. L. (1996). Calcite nucleation and precipitation kinetics as affected by dissolved organic matter at 25°C and pH > 7.5. Geochimica et Cosmochimica Acta, 60, 2765-2776.

Leturcq, G., Berger, G., Advocat, T., Vernaz, E. (1999). Initial and long-term dissolution rates of aluminosilicate glasses enriched with Ti, Zr and Nd. Chemical Geology, 160(1-2), 39-62.

781 Logan, W. S., Auge, M. P., Panarello, H. O. (1999). Bicarbonate, Sulfate, and Chloride Water in a
782 Shallow, Clastic-Dominated Coastal Flow System, Argentina. Groundwater, 37(2), 287-295.
783 Martínez, D. E., Quiroz Londoño, O. M., Solomon, D. K., Dapeña, C., Massone, H. E., Benavente,
784 M. A., Panarello, H. O. (2017). Hydrogeochemistry, Isotopic Composition and Water Age in
785 the Hydrologic System of a Large Catchment within a Plain Humid Environment (Argentine
786 Pampas): Quequén Grande River, Argentina. River Research and Applications, 33(3), 438-449.
787 Martínez, D., Bocanegra, E. (2002). Hydrogeochemistry and cation-exchange processes in the
788 coastal aquifer of Mar del Plata, Argentina. Hydrogeology Journal, 10(3), 393-408.
789 Ménard, O., Advocat, T., Ambrosi, J. P., Michard, A. (1998). Behaviour of actinides (Th, U, Np and
790 Pu) and rare earths (La, Ce and Nd) during aqueous leaching of a nuclear glass under
791 geological disposal conditions. Applied Geochemistry, 13(1), 105-126.
792 Morrás, H., Cruzate, G., (2000). Composición textural y distribución espacial del material
793 originario de los suelos de la Pampa Norte. XVII Congreso Argentino de la Ciencia del Suelo,
794 Mar del Plata, CD-ROM, 4 pp.
795 Nardi, A. de Vries, L.M. (2017). GibbsStudio, Barcelona Science Technologies SL, Barcelona,
796 Spain. Retrieved from http://gibbsstudio.io/
797 Nicolli, H.B., Bundschuh, J., García, J.W., Falcón, C.M., Jean, J-S. (2010). Sources and controls for
798 the mobility of arsenic in oxidizing groundwaters from loess-type sediments in arid/semi-arid
799 dry climates-evidence from the Chaco-Pampean Plain (Argentina). Water Resources, 44(19),
800 5589-604.
801 Nicolli, H.B., Suriano, J.M., Gómez Peral, M.A., Ferpozzi, L.H., Baleani, O.A. (1989). Groundwater
802 contamination with arsenic and other trace elements in an area of the Pampa, Province of
803 Córdoba, Argentina. Environmental Geology and Water Sciences, 14(1), 3-16.
804 Nicolli, H.B., Tineo, A., García, J.W., Falcón, C.M., Smedley, P.L. (2012). Mobilization of arsenic
805 and other trace element of health concern in groundwater from the Salí River Basin, Tucumán
806 Province, Argentina. Environmental Geochemistry and Health, 34(2), 251-62.

807 Nordeng, S. H. and Sibley, D. F. (1994). Dolomite stoichiometry and Ostwald's step rule.
808 Geochimica et Cosmochimica Acta, 58, 191-196.
809 Palandri, J.L., Kharaka, Y.K. (2004). A Compilation of Rate Parameters of Water-Mineral
810 Interaction Kinetics for Application to Geochemical Modeling. Geological Survey, California.
811 Paoloni, J.D., Fiorentino, C.E., Sequeira, M., Echeverría, N. (2002). Spatial variability and
812 concentration of Arsenic in the groundwater of a region in the southwest Buenos Aires
813 province, Argentina, Journal of Soil and Water Conservation, 55, 436-438.
814 Parkhurst, D. L., Appelo, C. A. J. (1999). User's guide to PHREEQC (Version 2): A computer
815 program for speciation, batch-reaction, one-dimensional transport, and inverse geochemical
816 calculations.
817 Paul, A. (1977). Chemical durability of glasses; a thermodynamic approach. Journal of Materials
818 Science, 12(11), 2246-2268.
819 Raychowdhury, A., Mukherjee, A, Bhattacharya, P., Johannesson. K., Bundschuh, J.,, Sifuentes,
820 G.B., Nordberg, E., Martin, R.A., Rosario-Storniolo, A. (2014) Provenance and fate of arsenic
821 and other solutes in the Chaco-Pampean Plain of the Andean foreland, Argentina: From
822 perspectivesof hydrogeochemical modeling and regional tectonic setting. Journal of
823 Hydrology 518, 300–316
824 Rinaldi, V. A., Rocca, R. J., Zeballos, M. E. (2007). Geotechnical characterization and behaviour
825 of Argentinean collapsible loess. Characterisation and Engineering Properties of Natural Soils,
826 2259-2286.
827 Rosen, O. M., Abbyasov, A. A., Tipper, J. C. (2004). MINLITH—an experience-based algorithm for
828 estimating the likely mineralogical compositions of sedimentary rocks from bulk chemical
829 analyses. Computers and Geosciences, 30(6), 647-661.
830 SAMLA (2004). Sistema de Apoyo Metodológico a los Laboratorios de Análisis de Suelo, Aguas,
831 Vegetales y Enmiendas Orgánicas: análisis de aguas. 1a edición. SAGyP. Dirección de
832 Agricultura. CD Rom.

833 Schultz, P. H., Zárate, M., Hames, B., Koeberl, C., Bunch, T., Storzer, D., Renne, P., Wittke, J.
834 (2004). The Quaternary impact record from the Pampas, Argentina. Earth and Planetary
835 Science Letters, 219(3-4), 221-238.
836 Scoppa, C. (1975). La mineralogía de los suelos de la llanura pampeana en la interpretación de
837 su génesis y distribución. Relatorio Actas VII. Reunión de la Asociación Argentina de la Ciencia
838 del Suelo, IDIA, Bahía Blanca, Suppl. 33.
839 Sifuentes, G. B. and Nordberg, E. (2003). Mobilisation of Arsenic in the Río Dulce Alluvial Cone,
840 Santiago del Estero Province, Argentina. MSc Dissertation, Department of Land and Water
841 Resources Engineering.
842 Smedley, P.L., Kinniburgh, D.G. (2002). A review of the source, behaviour and distribution of
843 arsenic in natural waters. Applied Geochemistry, 17, 517-568.
844 Smedley, P.L., Kinniburgh, D.G., Macdonald, D.M.J., Nicolli, H.B., Barros, A.J., Tullio, J.O. (2005).
845 Arsenic associations in sediments from the loess aquifer of La Pampa, Argentina. Applied
846 Geochemistry, 20(5), 989-1016.
847 Smedley, P.L., Nicolli, H.B., Macdonald, D.M., Barros, A.J., Tullio, J.O. (2002). Hydrogeochemistry
848 of arsenic and other inorganic constituents in groundwaters from La Pampa, Argentina.
849 Applied Geochemistry, 17, 259-284.
850 Smith, J., Vance, D., Kemp, R. A., Archer, C., Toms, P., King, M., Zárate, M. (2003). Isotopic
851 constraints on the source of Argentinian loess–with implications for atmospheric circulation
852 and the provenance of Antarctic dust during recent glacial maxima. Earth and Planetary
853 Science Letters, 212(1-2), 181-196.
854 So, H.U., Helle, U., Postma, D., Jakobsen, R.,, Larsen, F. (2008) orption and desorption of arsenate
855 and arsenite on calcite. Geochimica et Cosmochimica Acta, 72(24), 5871-5884
856 Steefel, C. I. and Van Cappellen, P. (1990). A new kinetic approach to modeling water-rock
857 interaction: The role of nucleation, precursors, and Ostwald ripening. Geochimica et
858 Cosmochimica Acta, 54, 2657-2677.

Techer, I., Advocat, T., Lancelot, J., Liotard, J. M. (2001). Dissolution kinetics of basaltic glasses: control by solution chemistry and protective effect of the alteration film. Chemical Geology, 176(1-4), 235-263.

Teruggi, M.E. (1957). The nature and origin of Argentine loess. Journal of Sedimentary Petrology, 27, 322-332.

Tófalo, O. R., Etchichury, M. C., Fresina, M. (2005). Textural and petrofacies characteristics of the Neogene deposits of Bancalari, Buenos Aires Province. Revista de la Asociación Geológica Argentina, 60, 316-326.

Vital, M., Martínez, D. E., Babay, P., Quiroga, S., Clément, A., Daval, D. 2019. Control of the mobilization of arsenic and other natural pollutants in groundwater by calcium carbonate concretions in the Pampean Aquifer, southeast of the Buenos Aires province, Argentina. Science of The Total Environment, 674, 532-543.

Weinzettel, P., Usunoff, E., Vives, L. (2005). Groundwater recharge estimations from studies of the unsaturated zone. Groundwater and Human Development. Balkema. Great Britain. Cap, 5, 133-143.

White, A. F. and Brantley, S. L. (1995). Chemical weathering rates of silicate minerals. Reviews in Mineralogy and Geochemistry, 31, 1-583.

Witkamp, M. (1966). Rates of carbon dioxide evolution from the forest floor. Ecology, 47, 492-494.

Zabala, M.E. (2014). El origen de la composición química del acuífero freático en la cuenca del arroyo del Azul (The origin of groundwater composition in the water-table aquifer of the Del Azul Stream basin). PhD Disseration. Facultad de Ciencias Exactas, Físicas y Naturales, Universidad Nacional de Córdoba, Argentina.

882 Zabala, M. E., Manzano, M., Vives, L. (2016). Assessment of processes controlling the regional
883 distribution of fluoride and arsenic in groundwater of the Pampeano Aquifer in the Del Azul
884 Creek basin (Argentina). Journal of Hydrology, 541, 1067-1087.
885 Zárate, M. A. (2003). Loess of southern South America. Quaternary Science Reviews, 22(18-19),
886 1987-2006.
887 Zinck, J. A., Sayago, J. M. (1999). Loess–paleosol sequence of La Mesada in Tucuman province,
888 northwest Argentina characterization and paleoenvironmental interpretation. Journal of
889 South American Earth Sciences, 12(3), 293-310.

Supporting information

Table S1. Chemical analyses (oxide weight %) of silicate glass in loess from different localities in the Chaco-Pampean Plain: A) Santiago del Estero, average of 13 samples (from Nicolli, 2010). B) Bell-Ville, Córdoba, 10 samples (from Nicolli, 1989). C) Centinela del Mar and Mar del Plata, Buenos Aires, 4 samples (from Schultz, 2003).

	RDA (A)	NLP (B)	MRAS (C)	Average	at % oxid
SiO_2	72.600	73.400	61.043	69.014	1.149
Al_2O_3	13.500	12.200	13.450	13.050	0.128
Fe_2O_3	0.830	0.650	5.490	2.323	0.015
FeO	0.620			0.620	0.009
MgO	0.720	0.170	3.313	1.401	0.035
CaO	1.180	1.030	4.723	2.311	0.041
Na_2O	4.010	3.420	4.210	3.880	0.063
K_2O	4.230	4.530	2.923	3.894	0.041
TiO_2	0.510	0.150	0.678	0.446	0.006
MnO	0.060	0.050	0.022	0.044	0.001
P_2O_5	0.060	0.040	0.845	0.315	0.002
lgn. loss	1.860	1.030	2.848	1.913	

Table S2. Chemical analyses of loess (as oxide weight %, and as element mol percentage, mol el. 100 g^{-1}) from different provinces in the Chaco-Pampean Plain: A: Santiago del Estero, average of 54 samples (from Nicolli et al., 1989). B: La Pampa, average of 45 samples (from Smedley et al., 2005). C: Buenos Aires Province, average of 6 samples (from González-Bonorino, 1965).

	RDA (A)		NLP (B)		MRAS (C)	
	wt % oxide	mol el.100 g^{-1}	wt % oxide	mol el.100 g^{-1}	wt % oxide	mol el.100 g^{-1}
SiO_2	59.69	0.993	64.1	1.067	63.16	1.051
Al_2O_3	15.03	0.295	14.6	0.286	19.66	0.386
Fe_2O_3	4.84	0.061	4.36	0.055	4.46	0.056
FeO	0.8	0.011	0.36	0.005		
MgO	1.85	0.046	2.06	0.051	1.47	0.036
CaO	6	0.107	2.47	0.044	2.02	0.036
Na_2O	2.68	0.086	2.38	0.077	2.37	0.076
K_2O	2.23	0.047	3.12	0.066	2.09	0.044
TiO_2	0.24	0.003	0.59	0.007	0.92	0.012
MnO	0.12	0.002	0.04	0.001		
CO_2					0.26	0.006
H_2O					4.23	

Table S3. Composition of 10 groundwater samples from the Del Azul Creek Basin used to calculate the equilibrium exchange constants.

GROUNDWATER SAMPLES: Del Azul Creek basin (Zabala et al. 2016)									
ID	Elevation (m asl)	Depth (m)	T (°C)	EC (µS/cm)	pH	Ca	Mg	Na	K
I1	130	30	15.8	899	7.9	10.3	2.8	182	8.1
I2	156	30	15.3	689	7.8	21	6.8	140.9	14.7
I3	169	30	15.1	656	7.7	33.6	12.5	99.3	17
I5	116	30	16.5	1100	7.5	33.5	15.5	203.2	21.4
I9	95	30	16.6	2920	7.2	70	36.2	567.9	25
I12	47	30	16.6	2820	7.4	75	65.4	478.5	39
I13	61	30	16.3	3850	7.6	27.4	29.2	825.9	30
I14	45	30	16.7	6440	7.2	99.2	84.1	1298	14.3
I15	82	30	16.5	1233	7.6	22.1	14.1	208.4	20.3
I20	159	30	15.5	730	7.6	27	14.1	125.1	22

Table S4. Total CEC and composition of the exchange complex of 15 sediment samples from the Del Azul Creek basin (in meq 100 g^{-1} soil).

SOIL SAMPLES: Del Azul Creek basin (Zabala et al. 2016)						
ID	Depth (m)	CEC	Ca	Mg	K	Na
I1A	6	20.7	23	6.6	1.5	2
I1B	20	29.7	27.5	7.9	1.8	3.4
I2	10	21.7	16.4	13.6	2	1.2
I3	22	23.1	23.2	9.5	1.6	1.2
I5	29	35.8	32.6	15.1	1.8	3
I9	29	33.2	31.1	12.5	1.9	4.1
I12	7	14.6	9.6	7	1.5	2.8
I13A	20	23	13.6	8.3	2	7.2
I13B	29	32.6	14.3	14.3	2.1	10.3
I14A	6	27	10.2	15.6	2.3	5.3
I14B	11	24.4	20.1	11.4	2.1	7.3
I14C	22	37.8	17.6	15.8	2.4	9.2
I15A	30	30.2	23.6	13.6	2.1	4.2
I15B	32	29.9	23.7	14.1	2	3.9
I20	3	11.3	10.2	6	1.3	0.6

Table S5. Measured chemical composition of groundwater samples from the Northern area of the la Pampa province (NLP) (from Smedley et al., 2002) and from Río Dulce Alluvial Aquifer (RDA) (from Benjarro and Nordberg, 2003). Units in mg L^{-1} except for Al and As, in µg L^{-1}. * Reported value below the analytical detection limit (4 µg L^{-1}).

Northern area of La Pampa Province (NLP) (Smedley et al., 2002)												
ID	Prof. (m)	pH	T (°C)	Ca	Mg	Na	K	HCO_3	Cl	Si	Al	As
962082	30	8.6	18.3	1.55	2.35	526	10.6	1270	12.5	27	250	4800
962083	20	8.2	18.8	4.15	7.97	695	15.9	1340	70	27	160	1800
962085	34.1	7.9	21	8.4	12.2	451	9.6	799	70	31	210	180
962090	131	8.0	26.4	10.2	7.93	233	10.9	258	150	22	27	8
962099	48	7.8	20.4	24.8	53	1360	25.6	635	970	28	640	210
970689	12	7.5	17.5	252	161	1320	16	518	1780	27	34	43
970700	14	8.1	18.6	5.43	8.25	692	14.8	1390	68.6	27	18	1400
970706	82	7.4	23.2	128	164	1520	36.4	536	1780	33	31	27
970783	26.9	7.0	20	599	521	2090	58.6	226	4580	31	10	<4*
970788	30	7.8	19.2	17.5	31.1	739	14.6	655	385	28	15	200
970797	94	7.5	26.7	30.5	37	546	19.8	497	513	35	9	220
970801	51	7.9	20.3	21	23.9	615	10.7	493	428	29	18	145
970808	28	8.3	19.8	4.23	11.4	882	14.4	1360	281	27	15	4900
970817	18.5	8.0	19	32.8	28.5	916	20.9	1440	248	27	38	2250
970820	25	8.1	18.4	7.78	15	1000	10	1360	409	26	20	520
Río Dulce Alluvial Aquifer in Santiago del Estero Province (RDA) (Benjarro and Nordberg, 2003)												
ID	Prof. (m)	pH	T (°C)	Ca	Mg	Na	K	HCO_3	Cl	Si	Al	As
CH47	7	7.3	23.5	2.1	0.6	261.1	5.7	479.2	51.9	30	6	170.1
SC8	3.5	7.4	24.8	5.7	2.4	441.1	12.7	754	89.3	21	8	1585.4
GP35	18	7.9	21.1	2.4	0.8	231.2	2.5	388.7	50.5	26	8.5	387.5
VG55	-	7.2		4.9	2	528.3	8.1	897.9	124.6	26	8	215.8
ESC19	5.5	7.7	22.7	87.2	14.5	129.3	17	452.9	53.7	22	7.8	237.8
JA41	6	7.2	21.6	74.8	25.9	106.9	90.2	440.7	80.6	28	10.3	838.7
MA7	4.5	7.2	23.6	20.9	5	225	11.8	396.8	70	26	10.8	23.5
LC58	6	7.5	21.1	3.2	0.8	383.1	7.3	584.2	113.1	17	27.9	98.5
SJ48	8	7.2	23	64.6	12.3	202.2	15.5	450.4	79.9	24	9.5	417.2
RR10	7.5	7.8	22.4	67.1	10.9	174.4	18.2	409	80.2	25	49.4	86.5
CR3	5	7.1	23.7	67	12.4	232.2	15	477.8	103.8	22	35.4	13494.1
EP38	7.5	6.9	22	92.1	20.7	262.3	24.1	588.5	132	25	16	27.6
CU6	9	8.7	23.5	53.7	9.5	282.5	15.7	490.9	117.8	26	10.6	33.9
ES51	7.5	7.2	22	88.9	19	182.4	17.9	486.5	91.2	26	15.9	34.2
CA2	7.5	7.2	22.6	56.9	16.2	295.1	21.8	552.9	113.8	25	12.5	41.4
TU52	7	7.5	22.3	77.7	18.4	204.2	37.7	484.6	113.9	28	16.4	74.7
ZP50	-	7.4	23.3	178	39.9	314.6	38.8	809.1	208.5	25	14.2	133.9
CG23	6	7.1	22.8	35.4	8.3	599.5	31.9	898.9	166.9	27	11.6	75.7
GA22	3.5	8.4	22.9	151.1	32.9	678.6	109.8	543.6	195.1	24	12.7	158.1
SJ56	-	6.9	2.6	55.3	9.6	429.1	16.6	657.4	175.3	26	18	389
LA20	4	7.4	23.3	92.9	15.2	160.2	22.3	443.1	71.2	15	15.3	100.1
NL31	1.9	6.9	21.3	82.3	15.4	133.3	14	385.5	89.6	17	32.5	86.3
GR36	6	7.2	21.7	97.5	22.9	208.4	45.2	468.5	148.2	28	13.3	92.1
EP28	7.5	7.0	22.7	44.2	17.1	492.5	44.6	759.3	201.6	29	18.4	60.4
ES59	10	9.0	22.1	59.7	12.7	269.1	18.4	415.8	165.8	24	15.3	355.4
PV33	5	8.2	21.5	75.4	14.1	138.3	38.1	338.7	73.3	23	12.1	43.8
TA18	8	7.3	23.4	3.8	0.8	381.8	5.1	432.4	172.3	25	12.4	40.8
TR46	3	7.3	22	52.7	8.9	119.8	15	258.9	59.3	21	16.1	21.2
13	6.5	7.5	22.7	118.3	17.4	154.6	59.8	421.2	138.5	21	12	24.4
MT57	8	7.4	2.5	5.7	2	409.5	7.5	451.9	165.5	19	12.1	15.5

Table S6. Calculated logartimic mineral saturation indices of groundwater samples from the Matanza-Riachuelo Aquifer System (MRAS) (this study), the Río Dulce Alluvial Aquifer (RDA) (from Benjarro and Nordberg, 2003), and from a Northern area of the la Pampa province (NLP) (from Smedley et al., 2002).

Matanza-Riachuelo Aquifer System in Buenos Aires Province (MRAS) (this study)							
ID	Andesine	K-Feldspar	Calcite	Illite	Ca-Mont.	Cinoenst.	Chalcedony
18F	-0.41	1.61	0.37	3.97	4.64	-3.18	-0.15
7F	0.15	2.36	0.31	4.92	5.16	-2.76	-0.20
24F	-	-	0.28	-	-	-2.90	0.13
15F	2.19	3.49	0.38	7.41	8.06	-2.72	0.07
2F	-0.64	1.68	0.37	3.40	3.57	-2.92	-0.27
22F	0.78	3.05	0.35	5.61	6.00	-2.68	0.11
12F	3.56	5.09	0.41	9.97	10.57	-2.64	0.29
23F	0.82	2.81	0.24	5.80	6.42	-3.06	0.05
32F	1.57	3.31	0.29	6.78	7.44	-2.73	0.13
11F	-0.16	2.12	0.53	4.35	4.74	-3.22	-0.14
36F	2.52	3.92	0.30	7.93	8.42	-2.58	0.08
25F	2.55	4.22	0.34	8.02	8.39	-2.35	0.17
17F	0.62	3.08	0.30	5.20	5.57	-2.49	0.25
19F	-0.23	2.05	0.62	3.83	4.12	-3.01	-0.12
27F	0.03	2.22	0.19	4.03	4.31	-2.42	0.03
20F	0.91	3.00	0.51	5.44	5.65	-2.21	0.09
30F	-	-	0.38	-	-	-1.99	0.27
35F	2.51	3.94	0.31	7.99	8.38	-2.69	0.02
Northern area of La Pampa Province (NLP) (Smedley et al., 2002)							
ID	Andesine	K-Feldspar	Calcite	Illite	Ca-Mont.	Cinoenst.	Chalcedony
962082	0.13	1.74	0.18	3.16	2.78	-1.88	-0.35
962083	-0.30	1.25	0.95	2.48	2.35	-1.97	-0.33
962085	-1.13	0.78	0.30	1.40	1.27	-2.30	-0.33
962090	0.15	1.75	0.25	3.47	3.26	-2.11	-0.34
962099	-0.98	0.59	0.42	1.38	1.33	-2.08	-0.35
970689	0.54	1.86	0.14	4.29	4.45	-2.40	-0.27
970700	-1.26	0.65	0.34	0.96	0.64	-1.81	-0.34
970706	-1.19	0.60	-0.08	1.63	1.68	-2.47	-0.42
970783	-0.97	0.96	0.08	2.09	2.34	-2.67	-0.21
970788	-0.94	0.76	0.25	1.80	1.85	-2.26	-0.31
970797	-0.80	0.75	0.31	1.82	1.91	-2.14	-0.30
970801	0.04	1.06	0.84	3.03	3.35	-2.25	-0.32
970808	1.51	2.60	0.29	5.70	5.63	-2.08	-0.31
970817	0.14	1.63	0.48	3.58	3.73	-2.36	-0.23
970820	-0.34	1.24	0.22	3.00	3.33	-2.73	-0.24
Río Dulce Alluvial Aquifer in Santiago del Estero Province (RDA) (Benjarro and Nordberg, 2003)							
ID	Andesine	K-Feldspar	Calcite	Illite	Ca-Mont.	Cinoenst.	Chalcedony
CH47	-2.18	0.02	0.26	-1.00	-1.36	-1.78	-0.32
SC8	-2.23	-0.41	0.54	-1.28	-1.73	-1.60	-0.52
GP35	-2.02	-0.07	0.01	-0.27	-0.21	-2.28	-0.32
VG55	-1.95	-0.18	0.17	-0.74	-0.80	-2.31	-0.39
ESC19	-2.39	-0.32	0.09	-0.74	-0.83	-2.81	-0.52
JA41	-0.89	1.15	0.50	2.15	2.18	-2.45	-0.31
MA7	-1.40	1.49	1.13	1.58	0.93	-1.53	-0.31
LC58	-1.84	0.41	0.28	0.45	0.30	-2.59	-0.41
SJ48	-1.63	0.36	0.08	0.63	0.78	-2.95	-0.32
RR10	-1.43	0.70	0.05	2.16	2.67	-3.64	-0.40
CR3	-1.53	0.89	0.28	1.94	2.19	-3.40	-0.39
EP38	-1.14	0.90	0.20	2.40	2.88	-3.58	-0.35
CU6	-1.87	0.21	0.43	1.44	1.84	-3.69	-0.57
ES51	-0.15	2.00	0.40	3.85	3.96	-3.11	-0.27
CA2	-1.01	1.06	0.50	2.60	3.00	-3.38	-0.34
TU52	-0.72	3.31	0.16	6.10	6.43	-4.62	-0.11
ZP50	-1.30	0.57	0.20	2.12	2.75	-3.82	-0.40
CG23	-0.46	1.49	0.30	3.08	3.37	-3.54	-0.32
GA22	-1.16	0.80	0.06	2.35	3.03	-3.97	-0.32
SJ56	-1.20	0.83	0.04	2.54	3.23	-4.05	-0.35
LA20	-1.25	0.86	0.15	2.32	2.83	-3.72	-0.33
NL31	-1.05	1.45	0.17	3.14	3.59	-3.82	-0.27
GR36	-1.08	0.86	0.02	2.78	3.53	-4.10	-0.35
EP28	-0.63	1.38	0.16	3.72	4.43	-3.94	-0.30
ES59	-1.52	0.67	0.10	2.45	3.22	-4.22	-0.39
PV33	-1.34	1.23	0.05	3.04	3.57	-4.39	-0.41
TA18	-0.98	0.95	0.02	2.75	3.52	-4.27	-0.31
TR46	-2.46	1.36	-0.73	4.28	5.59	-6.20	-0.27
13	-1.05	1.06	0.51	2.76	3.30	-3.80	-0.33
MT57	-1.20	1.22	-0.22	3.14	3.89	-4.52	-0.28